Lunar Descent Using Sequential Engine Shutdown

by

Philip N. Springmann

S.B., Aerospace Engineering

Massachusetts Institute of Technology (2004)

Submitted to the Department of Aeronautics and Astronautics
in partial fulfillment of the requirements for the degree of
Master of Science in Aeronautics and Astronautics
at the
MASSACHUSETTS INSTITUTE OF TECHNOLOGY
February 2006

Author .....
Department of Aeronautics and Astronautics
January 27, 2006

Certified by .....
Ronald J. Proulx
Principal Member of the Technical Staff
The Charles Stark Draper Laboratory, Inc.
Thesis Supervisor

Certified by .....
John J. Deyst
Professor of Aeronautics and Astronautics
Thesis Advisor

Accepted by .....
Jaime Peraire
Professor of Aeronautics and Astronautics
Chair, Committee on Graduate Students

Lunar Descent Using Sequential Engine Shutdown

by

Philip N. Springmann

Submitted to the Department of Aeronautics and Astronautics
on January 27, 2006, in partial fulfillment of the
requirements for the degree of
Master of Science in Aeronautics and Astronautics

Abstract

The notion of sequential engine shutdown is introduced and its application to lunar descent is motivated. The concept calls for the utilization of multiple fixed thrust engines in place of a single continuously throttleable engine. Downrange position control is provided by properly timed engine shutdowns. The principle advantage offered is the potential cost savings that would result from the elimination of the development cost of a throttleable rocket engine. Past lunar landing efforts are reviewed and provide the foundation for a baseline vehicle definition. A descent from a lunar parking orbit is assumed. The powered descent is divided into two phases, and a sequential engine shutdown-based guidance scheme is developed for the earlier phase. The guidance scheme consists of a biased ignition point and an algorithm for calculating shutdown times combined with a linear tangent steering law to provide full terminal position control. The performance of the sequential engine shutdown guidance scheme is assessed against two alternative approaches. A statistical picture of the performance of each guidance scheme is obtained via Monte Carlo trials of a lunar descent simulation that captures, to first order, the interaction between the descent propulsion system, the navigation filter, and the guidance function, allowing a direct comparison to be made on the basis of accuracy and fuel consumption. The impact of variations in the number of engines available in the sequential engine shutdown case is analyzed. While the performance observed with sequential engine shutdown does not match that observed with a throttleable engine, the results suggest that it is a viable solution to the lunar descent guidance problem.

Thesis Supervisor: Ronald J. Proulx
Title: Principal Member of the Technical Staff
The Charles Stark Draper Laboratory, Inc.

Thesis Advisor: John J. Deyst
Title: Professor of Aeronautics and Astronautics

Acknowledgments

This thesis was made possible by the generous support of the Charles Stark Draper Laboratory. I am grateful to Ron Proulx for his guidance, friendship, and willingness to sacrifice his own time in order to push my work forward. Tim Brand and Tom Fill were primarily responsible for the formulation of the sequential engine shutdown problem. Tom was also a constant and invaluable source of technical advice over the course of the project. Lee Norris kept an eye out for me from the day I arrived at Draper, and many others provided additional assistance and encouragement during my time there: Gregg Barton, Barbara Benson, Alisa Hawkins, Kevin Mahar, Steve Paschall, Anil Rao, George Schmidt, Jana Schwartz, Stan Shepperd, Y.-C. Tao, the Education Office staff, and the Technical Information Center staff.

I thank Professor John Deyst for his help not only with this thesis, but throughout my MIT career. I would also like to acknowledge Professor Olivier de Weck, who mentored me as an undergraduate research assistant. Thanks to Matt Richards for his help in proofing the manuscript.

Finally, I thank my parents, brothers, and sister for their love and support over the past six years. I cannot imagine having undertaken this work without them.

This thesis was prepared at The Charles Stark Draper Laboratory, Inc., under Internal Research and Development Project 20340-001, GC DLF Support.

1/27/2006

Philip N. Springmann — Date

Contents

List of Figures

List of Tables

Chapter 1

Introduction

Since serving as the focal point of the space race some forty years ago, the Moon has taken a back seat to other space exploration objectives, both manned and robotic. Against the backdrop of the Cold War, lunar exploration peaked in the 1960's and early 1970's, with numerous landing attempts made by Soviet Luna and American Ranger, Surveyor, and Apollo spacecraft. These early programs made great strides in trajectory design, propulsion, and guidance. While both Soviet and American robotic programs aimed for specific landing sites, according to their mission objectives, landing accuracy was by no means a primary concern. This changed with Apollo 12, which touched down near the previously landed Surveyor 3, accomplishing the first pinpoint landing on the Moon.

Following the Apollo and Luna landings, the space programs of both the United States and the Soviet Union turned to other efforts. The focus in manned spaceflight shifted to the Space Shuttle, Mir, and the International Space Station, while robotic spacecraft visited Mars and the outer planets. In the United States, the early 1990's saw a renewed interest in landing on the Moon, with NASA studying both robotic and manned lunar landings. More recently, the Bush Vision for Space Exploration has again placed a lunar landing on the list of national priorities. Any future lunar landing program is likely to have a fairly stringent requirement on landing accuracy, and will naturally aim to meet that requirement at a minimal cost. This is the context of the present thesis.

1.1 Historical Perspective

A timeline of every lunar landing ever accomplished is shown in Figure 1-1.* The first lunar landing occurred when Luna 2 impacted the Moon on September 14, 1959. Luna 2, along with the nearly identical Luna 1, represented the first of three families of Soviet Luna spacecraft. (Luna flights included both orbiters and landers.) Although Luna 2 released a sodium vapor cloud on its way to the Moon, so that it could be tracked visually, it had no propulsion system and thus made neither mid-course nor terminal maneuvers during its journey [1].

The year 1959 also saw the beginning of the Ranger program in the United States. The first two Ranger flights (Block I), launched in 1961, were intended to test systems and strategies for future lunar missions. Although neither spacecraft was placed on its planned deep space trajectory, they were able to demonstrate concepts like booster separation and solar panel deployment. In 1962, Ranger 3 was launched with the transmission of television pictures for ten minutes prior to lunar impact as its primary objective. Other mission features included a midcourse trajectory correction and a direct descent to the Moon with a terminal maneuver to slow the spacecraft prior to landing. To these ends, Rangers 3–5 (the spacecraft that comprised Ranger Block II) were equipped with liquid mono-propellant rocket engines for the midcourse maneuver and 22.5 kN solid rocket motors for the terminal maneuver. The planned terminal maneuver sequence for the Ranger Block II flights called for a series of pitch and yaw maneuvers to properly align the spacecraft, followed by deployment of a capsule containing scientific instruments, and finally solid motor ignition [2].

Due to an Agena upper stage guidance error, Ranger 3 missed the Moon completely. Ranger 4 was placed onto a trajectory that ensured lunar impact without a midcourse correction. However, its solar panels failed to extend and battery power was exhausted early in the flight. Ranger 4 impacted the far side of the Moon on April 26, 1962, the first U.S. spacecraft to land on the Moon. Ranger 5 lost power shortly after launch, precluding a midcourse correction, and missed the Moon [2].

*Figure 1-1 was adapted from an online source, "Lunar Exploration Timeline", by David R. Williams, http://nssdc.gsfc.nasa.gov/planetary/lunar/lunartimeline.html, accessed 9/9/2005.

Rangers 6–9 comprised Ranger Block III, and all had the primary objective of transmitting TV pictures of the lunar surface in support of the Apollo program. Each of these flights called for a midcourse correction as well as an active terminal maneuver to align the camera axis with the impact velocity vector. In the end, the midcourse maneuver was successfully executed on each of the Block III flights, while the terminal maneuver was successfully executed on Ranger 9 but cancelled on Rangers 6–8. Ranger 6 impacted the Moon but failed to transmit any imagery. Rangers 7–9 successfully achieved their mission objectives, and Rangers 7 and 9 impacted just a few miles from their original aim points [2].

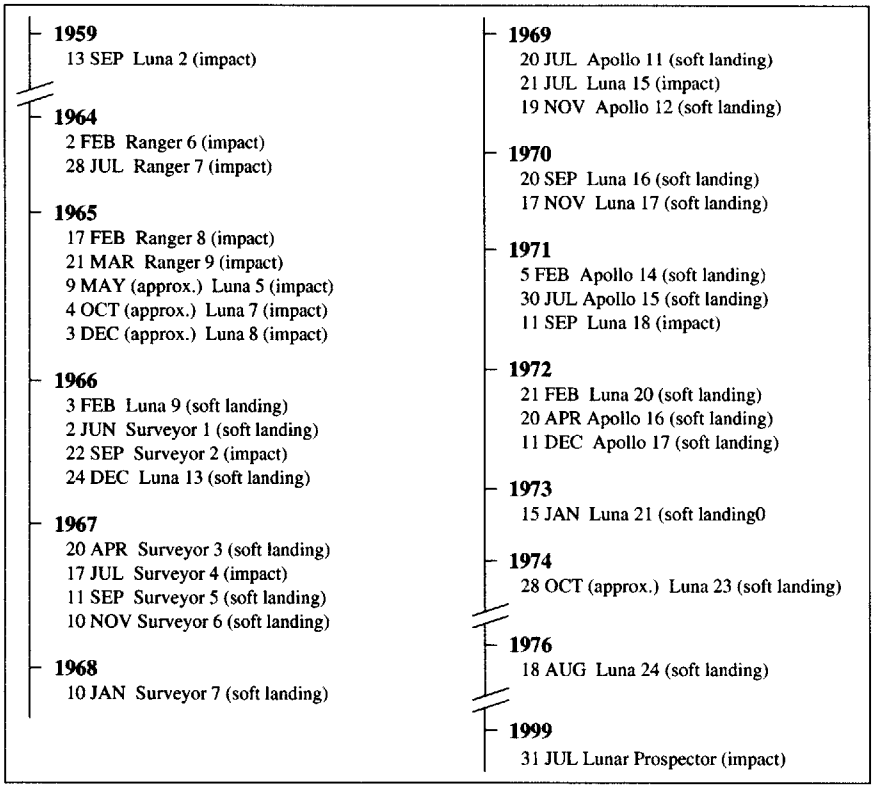

Figure 1-1: Lunar landing timeline

Shortly after the last Ranger flight, Luna 5 made an unsuccessful soft landing attempt and was followed by Lunas 6–8. (Lunas 5–14 made up the second family of Luna spacecraft. Lunas 10–12 were orbiters.) Luna 6 missed the Moon due to a failed midcourse correction, and Lunas 5, 7, and 8 all hit the Moon but failed to land softly due to failed or mistimed retro firings. Luna 9 achieved the first soft lunar landing

on February 3, 1966. Luna 13 matched the feat of Luna 9 later that same year [1].

The guidance scheme for these two craft was relatively simple. Lunas 9 and 13 coasted to the Moon along 3.5 day trajectories intersecting the Moon at approximately 0° N and 64° W. The key characteristic of this family of trajectories is that at 8,300 km altitude, a vector from the spacecraft to the center of the Moon is parallel to the approach hyperbola at the point where the approach hyperbola intersects the surface of the Moon, and the approach hyperbola is normal to the surface of the Moon at the point of intersection. Thus, Lunas 9 and 13 were aligned along a vector pointing at the center of the Moon at 8,300 km altitude, and that attitude was held for the remainder of the flight. As such, at the landing site, there were no local horizontal velocity components to null. Powered descent was initiated at approximately 75 km altitude. The engine was shut down when a ground contact probe indicated 5 m altitude, with the velocity between 4–7 m/s, and the payload was separated to ensure that it landed away from the spent propulsion unit [1].

Just four months after Luna 9, Surveyor 1 accomplished the first soft landing on the Moon by an American spacecraft. Surveyors 3, 5, 6, and 7 also successfully soft landed on the Moon between April 1967 and January 1968. While the payloads evolved over the course of the Surveyor program, the basic Surveyor bus and the direct trajectory it followed were essentially the same on each mission. The Surveyor 1 Mission Report [3] provides the relevant technical details of the program.

The Surveyor spacecraft used two descent propulsion systems. A single solid retrorocket motor with rated thrust between 35.5–44.5 kN provided the bulk of the braking capability. An additional vernier propulsion system consisted of three liquid rocket engines, throttleable between 135–460 N. The vernier system provided attitude control via differential throttling during the retrorocket burn, as well as velocity and attitude control during subsequent parts of the descent. A radar altimeter activated at 12.2 km altitude and a doppler velocity sensor provided altitude and velocity information along the descent.

The Surveyor landing maneuver consisted of a main retrorocket burn, a vernier phase, and a terminal sequence. Initially, the vehicle thrust axis was pointed along

a vector that was computed to be in the direction of the spacecraft velocity at main retrorocket ignition. The main retrorocket was ignited just after the spacecraft passed through 100 km altitude and burned at rated thrust for approximately 40 seconds, after which the remainder of the descent was made using the vernier engines.

The vernier phase began at an altitude between 3–15.3 km with the spacecraft velocity between 30–215 m/s. An acceleration of 0.9 lunar g was commanded until the *descent contour* was reached. The descent contour was a straight-line approximation to a precomputed parabolic altitude-velocity profile (see Ref. [3]). During the period of 0.9 g acceleration, the spacecraft held its original attitude until the velocity radar locked onto the lunar surface. The spacecraft then followed the descent contour with the thrust directed opposite the spacecraft velocity (i.e., a gravity turn) until just prior to touchdown.

The terminal sequence was initiated at approximately 12 m altitude. It consisted of a descent to 4 m altitude at a constant velocity of approximately 1.5 m/s, followed by a free fall to the surface. Surveyors 1 and 3 landed approximately 18.96 and 2.76 ± 1 km from their desired landing sites, based on lunar orbiter photos [4].

The Surveyor program, of course, helped pave the way for the Apollo lunar landings, though the propulsion and guidance systems on the Apollo lunar modules (LM) were far beyond their counterparts on the Surveyor landers. The Apollo LM descent propulsion system (DPS) had a rated thrust of 46.7 kN and could be operated at 93% of that value or throttled between 11% and 65% of rated thrust [5]. The specific impulse of the DPS was near 300 s [6].

Apollo powered descent was divided into three phases: the braking phase, the approach phase, and the terminal descent phase. From a near-circular lunar parking orbit at approximately 110 km altitude, the lunar module was transferred to an elliptical coasting orbit, and the braking phase was initiated near perilune at approximately 15 km altitude. The braking phase was initiated with the lunar module approximately 492 km uprange of the landing site. The braking burn lasted approximately 514 s, and was near-optimal with respect to fuel consumption [5].

The standard approach to the development of a near fuel-optimal guidance law for

a vehicle with a throttleable engine begins with a simple variational problem, namely, to find the acceleration history $\mathbf{a}(t)$ that minimizes the functional

$$J = \int_{t_0}^{t_f} \mathbf{a}^T(t)\mathbf{a}(t)\, dt \tag{1.1}$$

where $\mathbf{a}(t)$ is the total acceleration vector, the equations of motion are

$$\frac{d\mathbf{r}}{dt} = \mathbf{v}\,, \quad \frac{d\mathbf{v}}{dt} = \mathbf{a} \tag{1.2}$$

and the boundary conditions are

$$\begin{matrix} \mathbf{r}(t_0) = \mathbf{r}_0 \\ \mathbf{v}(t_0) = \mathbf{v}_0 \end{matrix} \quad \text{and} \quad \begin{matrix} \mathbf{r}(t_f) = \mathbf{r}_f \\ \mathbf{v}(t_f) = \mathbf{v}_f \end{matrix} \tag{1.3}$$

as outlined in Ref. [7].

The explicit guidance law for the Apollo LM braking phase, known as E guidance, was indeed based on the solution to this problem, and in its simplest form can be written

$$\mathbf{a}(t) = \frac{12}{t_{go}^2}(\mathbf{r}_f - \mathbf{r}) + \frac{6}{t_{go}}(\mathbf{v}_f + \mathbf{v}) + \mathbf{a}_f \tag{1.4}$$

In the actual guidance implementation, Equation (1.4) contained multiplicative terms to account for computation time [5]. To prevent unbounded gains in the explicit guidance equation, the braking phase target was a point 541 m below the lunar surface and 4.4 km uprange of the landing site, with the desired initial conditions for the approach phase obtained along the path to this false target.

The approach phase began at approximately 2.2 km altitude and 7.5 km uprange of the landing site. This phase lasted approximately 146 s and was designed to provide continuous visibility of the landing site, albeit at the expense of fuel consumption. The approach phase was terminated almost directly above the landing site — 30 m altitude, 11 m uprange — at which point the terminal descent phase began. During the terminal descent phase, forward and lateral velocity components were nulled out, and the altitude rate of the lunar module was controlled until touchdown [5].

Luna 15, the first of the so-called "heavy" Luna spacecraft, was the next Luna mission to fly after Luna 13, and was launched just three days before Apollo 11. It failed to achieve a soft landing and impacted the lunar surface after 52 orbits of the Moon [1]. Subsequent missions were more successful. Between 1970 and 1976, Lunas 16, 20, and 24 accomplished robotic sample return missions, and Lunas 17 and 21 carried rovers to the surface of the Moon.

The heavy Luna landers all followed similar flight plans. After an approximately 4.5 day journey to the Moon, the spacecraft was inserted into a near-circular lunar parking orbit with an altitude between 90–115 km. From this parking orbit, the lander was transferred to an elliptical orbit with a perilune between 15–20 km altitude. A retrorocket firing over the landing site nulled the horizontal velocity and sent the lander into a vertical drop toward the surface of the Moon. At 760 m altitude, with a velocity of 200 m/s, the descent engine was re-ignited, and slowed the spacecraft to a descent rate of 2.5 m/s at 20 m altitude. At that point, braking was switched to two secondary thrust chambers to minimize disturbances to the soil at the landing site [1].

By the time the heavy Luna spacecraft were flown, attention within the U.S. space program had turned to the Space Shuttle. While the Space Shuttle itself had nothing to do with landing on the Moon, its ascent guidance routine can be applied to the lunar landing problem. The second stage ascent guidance algorithm on board the Shuttle, known as Powered Explicit Guidance (PEG), is a mechanization of the solution to the classic minimum-time orbit injection problem. Both the minimum-time orbit injection problem and Powered Explicit Guidance are covered with the requisite mathematical detail in Chapter 3.

Shuttle ascent guidance and lunar descent guidance are similar in that both are designed to transfer a vehicle from an initial position and velocity to some desired altitude and velocity, so it follows that the guidance routine for one application might be adapted to the other. They differ, though, in that on a Shuttle ascent, the down-range position at which the final altitude and velocity are achieved is unimportant. On ascent, the Shuttle generally follows a thrust acceleration profile that is specified

a priori, and the downrange position at cutoff is fixed by the boundary conditions of the ascent trajectory and the thrust acceleration profile. However, the Space Shuttle Main Engines (SSME) are throttleable, and the Shuttle guidance function is capable of adjusting the throttle setting to control the final downrange position.

The most recent NASA proposals involving a lunar landing — prior to the announcement of the Bush Vision for Space Exploration — were developed in the early 1990's, and relied on PEG for lunar descent guidance. PEG is well-suited to lunar descent guidance because it is near fuel-optimal, computationally efficient, and — given a throttleable propulsion system — can fully control the final position and velocity of the lander. While not mentioned explicitly, its application to lunar descent is outlined in Ref. [8].[†]

The descent strategy consisted of three phases: a powered descent phase, a pitch-up phase, and a landing phase. The pitch-up phase is necessary because the commanded vehicle attitude on a PEG-guided descent remains nearly horizontal throughout the burn. The powered descent phase, which covered the bulk of the burn, was PEG-guided with its target biased to account for position and velocity changes anticipated over the pitch-up maneuver. The pitch-up phase consisted of a constant rate pitch-up combined with a linear throttle down to bring the vehicle to a vertical attitude while slowing the descent rate. The landing phase nulled all forward and lateral velocity components and took the vehicle through a controlled drop to a soft landing on the surface of the Moon.

1.2 Problem, Approach, and Objective

A decade later, with a new presidential mandate, NASA is again looking toward the Moon. Early indications are that the lunar Crew Exploration Vehicle (CEV), as it is known, will be an Apollo-like spacecraft, albeit much bigger. Few technical details of the new lunar missions have been released. However, it would be reasonable to

[†]The powered descent concept outlined in this reference was developed for a proposed program known as First Lunar Outpost.

speculate that, as in all past lunar landing efforts where accuracy has been a concern, a throttleable descent propulsion system will be part of the vehicle design.

Because the cost associated with the development of throttleable rocket engines is quite high, it may be possible to realize some cost savings by substituting multiple constant thrust engines for a single throttleable one. In light of this possibility, the present thesis develops and evaluates a guidance scheme for a lunar landing vehicle equipped with several constant thrust engines. (The guidance scheme does not depend on a particular number of engines.) Such a vehicle, rather than being able to produce any arbitrary level of thrust over a given range, is capable only of a certain number of discrete *thrust levels*.

This thesis assumes a lunar descent strategy divided into two phases. The first, henceforth known as the *braking phase*, includes the portion of the powered descent between ignition and the time the vehicle reaches 1–2 *km* altitude. The second phase, referred to as the *terminal descent phase*, covers the remainder of the descent.[‡] While the terminal descent phase is accounted for in Chapter 2, this thesis is concerned with braking phase guidance.

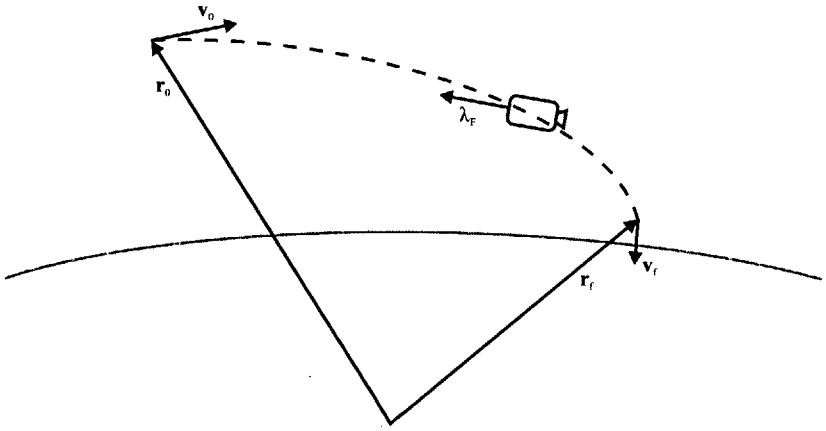

Figure 1-2: Braking phase guidance problem

The braking phase guidance problem is a two-point boundary value problem and is diagrammed in Figure 1-2. The landing vehicle has some initial position and velocity and is to be brought to a final position and velocity from which the terminal descent

[‡]The term *terminal descent phase*, as used here, includes any maneuvers bridging the braking phase and the final descent, such as the *pitch-up phase* described toward the end of Section 1.1.

is commenced. Nominally, the braking phase target lies in the orbital plane of the vehicle. The braking phase target typically consists of a small radially downward velocity at an altitude several kilometers above the landing site, allowing for a divert maneuver as necessary followed by a vertical descent to the surface of the Moon.

The landing vehicle can be defined for the purposes of this thesis by its initial thrust-to-weight ratio F/m_0, initial mass m_0, and specific impulse I_{sp} (or exhaust velocity v_{ex}, since $v_{ex} = I_{sp}g_0$, where g_0 is the acceleration due to gravity at the surface of the Earth). Several assumptions regarding the landing vehicle are necessary to completely define the problem of this thesis and are stated here:

1) *All engines have the same thrust rating and cannot be throttled.*

Given this assumption, a vehicle's thrust levels are a function of its maximum thrust — itself determined by the initial thrust-to-weight ratio and vehicle mass — and the number of engine pairs (see item 3 below) it carries. For example, if the vehicle has a maximum thrust of 9 kN and 3 engine pairs, its thrust levels are 9 kN, 6 kN, and 3 kN.

2) *The descent is initialized with all engines on, and each engine can be shut down only once during the braking phase.*

This statement is the source of the term *sequential engine shutdown.* Descending at a higher thrust level is more fuel efficient than descending at a lower thrust level, so the descent is initialized at maximum thrust. Also, the type of engine implicitly assumed in this thesis is not generally designed to be started and stopped at will. Therefore, the worst case is assumed and engines are not allowed to be restarted once they have been shut down.

3) *Engines are shut down in pairs to change the thrust level.*

When paired, the engines can be arranged on the vehicle such that the net thrust is maintained through the vehicle's center of gravity at all times.

The usual objective in solving the braking phase guidance problem is to obtain a

control that minimizes fuel consumption (i.e., ΔV). If the vehicle is capable of variable thrust, a variational problem can be solved for the minimum-fuel thrust acceleration vector history that satisfies the boundary conditions, as laid out by Battin [7] and D'Souza [9]. This was alluded to in the discussion of Apollo descent guidance in Section 1.1.

The optimal control law for a powered ascent or descent under a flat Earth assumption, if the vehicle's thrust acceleration history is specified *a priori* (for example, in the case of a fixed thrust vehicle) and the final downrange position is unimportant, is a bilinear tangent law. Under these conditions, the downrange component of the final position is fixed by the boundary conditions and the thrust acceleration history. With a throttle, it becomes possible to change the thrust acceleration history on the fly and thereby control the final downrange position; the lower the throttle setting, the greater the final downrange position.

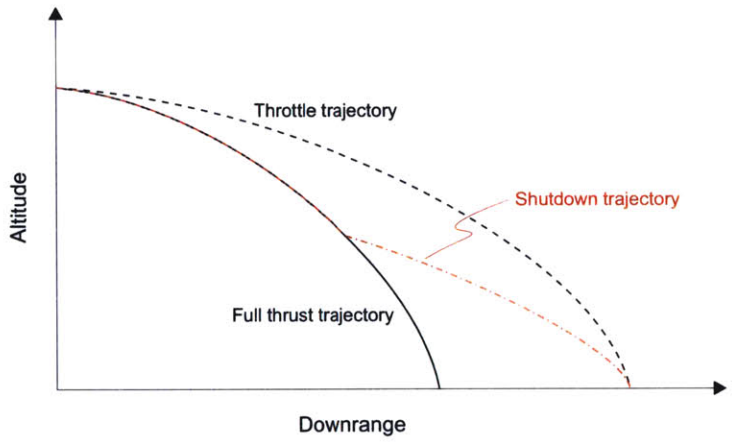

Figure 1-3: Notional throttle and engine shutdown trajectories

A properly timed reduction in the thrust setting, realized by shutting down an engine pair, can produce the same result, as illustrated conceptually in Figure 1-3. The *shutdown time* can be adjusted like the throttle setting to achieve a desired final downrange position; the earlier the shutdown, the greater the final downrange position. Fundamentally, an adjustment to a throttle setting or shutdown time modifies the thrust acceleration history such that the desired final downrange position is achieved. Of course, unlike a throttle, which can be adjusted up or down at any

time, a shutdown is a one-way control. If vehicle performance is nominal and the navigation solution is perfect, a single shutdown is all that is needed to control downrange position, and the computation of the shutdown time is trivial. However, with off-nominal thrust, specific impulse variations, and navigation uncertainty present, and multiple shutdowns possible, the development of a slightly more sophisticated shutdown strategy is required.

The objective of this thesis is the development and evaluation of a sequential engine shutdown algorithm aimed at reducing dispersions in vehicle position and velocity at the end of the braking phase. The overall guidance strategy relies on PEG for thrust direction (steering) commands, and the shutdown algorithm gives the thrust magnitude history. Shutdown algorithm development centers on control of the final downrange position, since the PEG steering law provides control of all other components of the final state. The shutdown algorithm fits into the overall guidance scheme as shown in Figure 1-4.

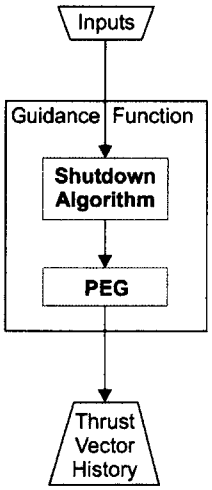

Figure 1-4: Sequential engine shutdown guidance scheme block diagram

This thesis is organized into five chapters. The remainder of the present chapter motivates the thesis problem and reviews the published literature relevant to it. The first part of Chapter 2 introduces a baseline vehicle and a reference mission, which together comprise a design point for the shutdown algorithm. The rest of Chapter 2 provides a first look at the use of sequential engine shutdown and explores the sensi-

tivity of vehicle performance to changes in the baseline vehicle definition and reference mission.

Chapter 3 describes a braking phase guidance strategy for a sequential engine shutdown vehicle, beginning with a review of the optimal control problem underlying PEG and a derivation of the PEG equations. The relationship between throttling and engine shutdowns for terminal downrange control is discussed, and a shutdown algorithm is developed. An evaluation of the guidance strategy is contained in Chapter 4, including an assessment of its performance versus that obtained with both fixed thrust and a throttle. Conclusions and recommendations for future study are presented in Chapter 5.

1.3 Motivation

The importance of landing accuracy is easily established. An accurate[§] lunar (or planetary) landing allows the landing vehicle to land near a previously landed spacecraft, such as an astronaut habitat. Scientific objectives can rely on a spacecraft reaching a specific landing site. If a landing area can be surveyed prior to the arrival of the landing vehicle, higher landing accuracy ensures a lower probability of a hazard encounter.

From a system architecture perspective, use of sequential engine shutdown expands the lunar landing vehicle design space. Vehicle architectures relying on sequential engine shutdown can be characterized in terms of cost, required development time, and performance. This section argues that sequential engine shutdown shows enough promise with respect to these metrics to justify its development in this thesis. The argument for sequential engine shutdown is premised on the fact that the technique permits an acceptable level of downrange position control. There are some practical difficulties, but in principle, adjusting a shutdown time offers the ability to control downrange position in much the same way as adjusting the throttle setting.

Sequential engine shutdown is attractive primarily because of the possible cost

[§]What constitutes an *accurate* landing is mission-specific.

savings it offers over a continuously throttleable engine. That cost savings would result from the elimination of the development cost of a new throttleable rocket engine. One 1997 figure shows that the development cost of a new rocket engine can be as high as $3 billion over the course of nearly a decade [10]. The Space Shuttle Main Engine (SSME) is the most relevant current example of a throttleable rocket engine, with the ability to throttle between 65–109% of its 2.09 MN rated thrust. The SSME is the most advanced rocket engine ever built, and it is expensive. As of 1996 the SSME contract had a total value in excess of $5.6 billion [11].

It can also be argued that variable thrust engines are susceptible to performance losses that stem directly from their throttling capability. The thrust generated by a rocket engine is directly proportional to its chamber pressure. Throttling of a liquid rocket engine is accomplished by reducing the propellant flow supply to the thrust chamber, thereby lowering the chamber pressure. A consequence is a small decrease in specific impulse, implying reduced fuel efficiency. Thus, there is a performance penalty, albeit a small one, inherent in a throttleable engine [12] (Ref. [12] even notes multiple constant or slightly variable thrust engines as an alternative to a throttleable engine). This is a weak argument, however, as in almost all cases, the increased ΔV required for sequential engine shutdown offsets the small losses incurred as a result of throttling.

In terms of ΔV, the most efficient way to reach a particular downrange position using PEG is to maintain a constant thrust setting throughout the burn. The same downrange position can be achieved by transitioning from a high thrust level to a lower one during the burn, the result of which is an equivalent "average" thrust setting over the burn. The latter technique, though, requires a higher ΔV. The greater ΔV requirement is the principal performance disadvantage of sequential engine shutdown.

Additionally, the higher ΔV requirement could be exacerbated by mass inefficiencies resulting from a multiple engine configuration. It is conceivable that the propulsion system dry mass might be higher for a multiple constant thrust engine configuration that for a single throttleable engine. This, in turn, would require the vehicle to carry more fuel to achieve the same ΔV. A multiple engine configuration

also introduces previously non-existent susceptibility to off-nominal engine performance. A thrust differential between two engines would create a moment about the center of gravity of the vehicle which would have to be nulled out.

Finally, sequential engine shutdown is a one-way control. According to the assumptions outlined in Section 1.2, an engine cannot be restarted once it has been shut down. Thus, with each shutdown some ability to adjust the final position uprange is lost. This is one of the main practical difficulties with sequential engine shutdown, but does not present an insurmountable hurdle.

1.4 Literature Review

Naturally, the formative work in optimal lunar descent guidance parallels the pre-Apollo and Apollo programs. This includes the original derivation of the linear tangent law published in 1963 by Lawden [13], and the development of the E guidance method for the Apollo lunar module by Cherry and others [14]. A more recent publication is the 1999 development of a near-minimum fuel guidance law for the Japanese Selene mission by Ueno and Yamaguchi [15]. Termed *polynomial guidance*, the guidance law is similar to that generated by PEG, with the thrust elevation angle obeying a linear tangent law and the thrust azimuth angle constant. This follows logically since the terminal velocity is constrained but the landed position is not. Since the derivation assumes constant thrust acceleration, no iteration is necessary; the burn time and thrust direction history can be calculated directly.

A 2002 paper by Axelrod, Guelman, and Mishne [16] solves the optimal control problem for an interplanetary spacecraft using electric propulsion with discrete thrust levels. The optimal thrust direction is the direction of the primer vector, a result equivalent to a three-dimensional linear tangent law. The optimal thrust level at any given time is the available thrust level closest to the magnitude of the primer vector. This is consistent with the assertion in the present thesis that the fuel-optimal thrust magnitude history for a single-shutdown descent includes the nearest thrust levels on either side of the constant thrust level that would yield the desired final downrange

position using PEG. However, Axelrod, et. al., assume that the thrust level can be adjusted up or down at any time.

Demonstrating the optimality or near-optimality of a guidance method is difficult because the simplifying assumptions made in order to derive the guidance equations — typically a flat Earth and constant gravity, and sometimes constant thrust acceleration — do not hold under real operating conditions. Thus, there is a large body of work dealing with the numerical optimization of space trajectories according to various criteria, some of which specifically focuses on lunar landings. Recent examples include optimizations of lunar descents from parking orbits by Vasile and Floberghagaen [17] and by Hawkins [18]. The former optimization is based on a cost function involving the square of the control input, while the latter takes a minimum fuel approach.

One formulation of the trajectory optimization problem of particular relevance to the present thesis is that in which the covariance of the state estimate error is included in the cost function. Zimmer, Ocampo, and Bishop [19, 20] have developed a method of solving trajectory transfer problems while minimizing a combination of fuel consumption and final state uncertainty. The result is a trajectory that differs slightly from the fuel-optimal trajectory so that measurement quality is improved. An analogous terrestrial concept would be something like a path planning algorithm that minimizes the geometric dilution of precision of GPS measurements. The technique can be applied to minimize the covariance associated with specific states not necessarily expressed with respect to a Cartesian coordinate frame, such as semi-major axis or flight path angle [21]. The present thesis work takes the covariance profile over the descent as fixed. Rather than attempt to fly a trajectory that minimizes the covariance of the state estimate error at landing, engine shutdowns are planned such that the ability to reach the desired final position is preserved while the covariance of the state estimate error decreases along the descent trajectory.

Chapter 2

Using Sequential Engine Shutdown

Understanding the performance characteristics of a vehicle using sequential engine shutdown is the first step toward development of a guidance strategy. Since the key performance measures (i.e., burn time, ΔV requirement, and final downrange position) are dependent upon certain vehicle properties, it is necessary to define a baseline vehicle as well as the initial conditions for the braking phase, so that the these measures can be quantified. The baseline vehicle and a reference mission — which determines the initial conditions for the braking phase — are defined in the first part of this chapter.

The second part of the chapter looks at how burn time, ΔV, and final downrange position vary as functions of shutdown time. It also looks at how these quantities are affected by changes to the baseline vehicle definition. Of particular note are the effects of shutdown timing and certain vehicle properties on the range of achievable final downrange positions. Development of the shutdown algorithm in Chapter 3 follows directly from the analysis in Section 2.3. The later sections of this chapter, particularly Section 2.3, are meant to lend an intuitive feel for the level of control authority provided by sequential engine shutdown and the effects of shutdown timing.

2.1 Baseline Vehicle

The characteristics of the landing vehicle relevant to the guidance strategy are its initial thrust-to-weight ratio F/m_0 and specific impulse I_{sp}, which determine the thrust acceleration profile over the burn, as well as the number of engine pairs on board. A baseline vehicle mass is specified as well, mainly to add relevance in view of NASA's recently announced lunar exploration system architecture, and to allow quantities such as fuel consumption to be extrapolated from the data in Chapter 4. The baseline vehicle definition is based on trends in actual and hypothesized lunar landing vehicles dating from the Apollo era to the present. These vehicles are listed in chronological order in Table 2.1.*

Table 2.1: Actual and hypothesized lunar landing vehicles

	F/m_0 (N/kg)	F_{max} (N)	m_0 (kg)	I_{sp} (s)
Apollo LM [5, 6]	3.06	45,040	14,719	300
Heavy Luna [1]	4.89	18,044	3,690	N/A
Common Lunar Lander	3.22	3,430	1,066	341
First Lunar Outpost	3.92	293,568	74,890	444
Moonrise Vehicle	3.24	7,117	2,200	315
Hawkins Thesis Vehicle [18]	4.44	8,000	1,800	358
Draper/MIT CEV Study [22]	3.20	202,000	63,282	462

Moonrise, a proposal involving a landing near the Moon's south pole, was tabbed as a candidate for the next mission in NASA's New Frontiers Program in 2004. A notable feature of the conceptual vehicle design was a descent propulsion system consisting of eight large thrusters of equal size. The idea of shutting these thrusters down in pairs to control downrange dispersions received some preliminary study, which provided some of the impetus for this thesis.

Although Table 2.1 contains just seven records — with distinct mission objectives underlying each one — it is possible to make some limited inferences from it. Robotic vehicles are generally much smaller than their manned counterparts, since they do

*Entries without accompanying citations are based on data provided by Gregory Barton and Thomas Fill of the Charles Stark Draper Laboratory. The m_0 and I_{sp} values for Common Lunar Lander are estimates.

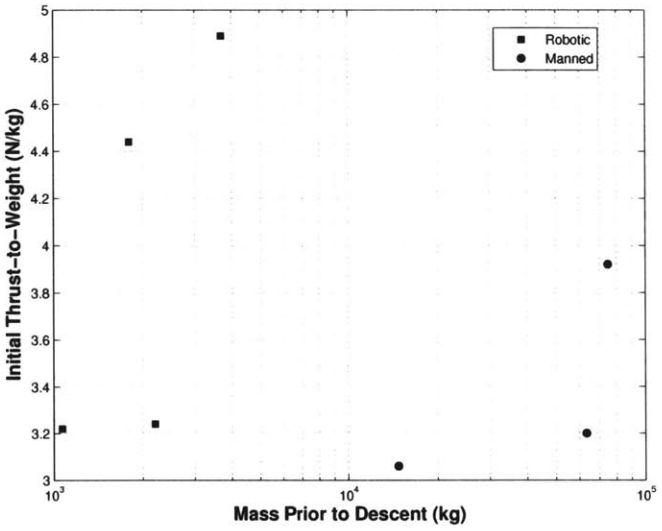

Figure 2-1: Lunar landing vehicle design space

not support a multiple person crew, and thus typically have higher thrust-to-weight ratios than manned vehicles. This is indicated in Figure 2-1, which locates the vehicles listed in Table 2.1 in a sort of "design space". Also, specific impulse has increased substantially over the years. This is reflected in the inclusion of descent engines fueled by liquid hydrogen and liquid oxygen in the First Lunar Outpost and Draper/MIT CEV [22] conceptual designs versus the Aerozine 50/50 and nitrogen oxide used by the Apollo LM descent propulsion system.

The baseline vehicle definition for this thesis is given in Table 2.2. It is intended to reflect the anticipated lunar Crew Exploration Vehicle (CEV)[†] design, which implies a fairly large vehicle, a moderate initial thrust-to-weight ratio, and a high specific impulse. This is the definition used to produce the data presented in Chapter 4.

Table 2.2: Baseline vehicle definition

	F/m_0 (N/kg)	F_{max} (N)	m_0 (kg)	I_{sp} (s)
Baseline	3.50	227,500	65,000	440

It is necessary to impose one additional requirement that affects the number and magnitude of the thrust levels available during the braking phase. Namely, the lowest

[†]A preliminary description and artist's concept of this vehicle are available from NASA's web site, http://www.nasa.gov/mission_pages/exploration/spacecraft/index.html, accessed 1/9/2006.

available thrust level must produce an acceleration that exceeds that of lunar gravity, preserving the option of an abort. This condition does not have to hold over the entire braking phase, but it must exist by the earliest time in the descent at which it would be reasonable to expect that the vehicle might be operating at the lowest available thrust level.

Given this requirement, the number of available thrust levels is not simply the number of engine pairs on the vehicle. However, calculating the number of available thrust levels and their magnitudes is straightforward. The number of engine pairs must be a positive integer, which is also the maximum number of available thrust levels. The maximum thrust level is known, and the minimum thrust level must be such that it will produce a thrust acceleration which exceeds that of lunar gravity some time into the braking phase. Since acceleration is thrust divided by mass, an estimate of the largest mass with which the vehicle might operate at its lowest thrust level is required.

This mass estimate can be produced as follows. First, the earliest realistic time t_1 at which the lowest thrust level might be commanded must be estimated. This estimate can be made using the analysis presented in the next section. The minimum ΔV required along the descent between $t = 0$ and $t = t_1$ is given by

$$\begin{aligned} \Delta V_1 &= \int_0^{t_1} \frac{F_{max}}{m_0 - \dot{m}t}\, dt \\ &= -v_{ex} \ln\left(1 - t_1/\tau\right) \end{aligned} \tag{2.1}$$

where $\tau = \frac{v_{ex}}{F_{max}/m_0}$. The vehicle mass after achieving this ΔV is

$$m_1 = m_0 \frac{1 - e^{(\Delta V_1/v_{ex})}}{e^{(\Delta V_1/v_{ex})} - 1} \tag{2.2}$$

and is the maximum possible mass the vehicle can have when the lowest thrust level is commanded. Thus, the lowest thrust level must be greater than $m_1 g_M$, where g_M is the acceleration due to gravity near the surface of the moon.

With the minimum allowable thrust setting known, the number of available thrust

levels and their magnitudes can be easily calculated for a given number of engine pairs. The possible thrust levels range from the thrust provided by a single engine pair to the maximum thrust, in uniform intervals. The lowest *available* thrust level F_{min} is simply the lowest of those thrust levels that exceeds the minimum allowable thrust setting. Table 2.3 shows the available thrust levels for various numbers of engine pairs assuming the baseline vehicle definition and $t_1 = 300\ s$. By inspection of Table 2.3, it is easy to see how many thrust levels are provided by a given number of engine pairs, or inversely, how many engine pairs are necessary to provide a desired number of thrust levels.

Table 2.3: Available thrust levels by number of engine pairs

Avail. Thrust Levels	F_{max} (N)	F_{min}	*Engine Thrust*	*No. Engine Pairs*
1	227,500	227,500	113,750	1
2	227,500	113,750	56,875	2
2	227,500	151,666	37,916	3
3	227,500	113,750	28,437	4
4	227,500	91,000	22,750	5
4	227,500	113,750	18,958	6
5	227,500	97,500	16,250	7
6	227,500	85,312	14,218	8
6	227,500	101,111	12,638	9
7	227,500	91,000	11,375	10

Although not dealt with in this thesis, the terminal descent is a major driver in evaluating the utility of each configuration listed in Table 2.3. For example, even if only two thrust levels were needed for the braking phase, the lower thrust level may not be appropriate for the terminal descent. The terminal descent could conceivably require additional thrust levels below the minimum level available for the braking phase, which some of the configurations with more engine pairs provide.

2.2 Reference Mission

The performance measures of interest in this chapter are also affected by the initial conditions for the braking phase. These initial conditions are in turn a function of

the mission architecture, which determines the path followed by the vehicle to the Moon. There are three somewhat standard Earth-Moon trajectories. The simplest is a direct descent like those flown by the Ranger and Surveyor probes. The direct descent is efficient in terms of ΔV but limits the location of the landing site. A second option is to enter a lunar parking orbit prior to the descent to the surface. A short burn places the vehicle in an elliptical coasting orbit from which powered descent is initiated. This was the approach taken by the Apollo and heavy Luna landers, all of which utilized similar parking and transfer orbits. A third possibility is to initiate lunar descent from the L_1 Earth-Moon libration point. This approach might prove feasible for missions aimed at establishing and re-supplying a permanent presence on the Moon, but is unlikely to be used in the 10–20 year time frame.

Given its Apollo and Luna heritage and the likelihood that it will be a part of the next manned moon landing, an approach from a lunar parking orbit is assumed in this thesis. The altitude of the parking orbit, perilune altitude of the transfer orbit, desired altitude at the end of the braking phase, and desired sink rate (i.e., radially downward velocity) at the end of the braking phase define the so-called reference mission. The values of the reference mission parameters used in this thesis are listed in Table 2.4.

Table 2.4: Reference mission parameters

Parameter	*Value*	*Units*
Parking Orbit Altitude	100.0	km
Transfer Orbit Perilune	17.5	km
Target Altitude	1.5	km
Terminal Sink Rate	1.0	m/s

Target altitude refers to the desired altitude at the end of the braking phase. On a nominal descent the vehicle should be able to make a vertical descent from this altitude to the landing site. The target altitude is left relatively high, however, to account for the possible need to re-designate the landing site and divert from the vertical descent.

The reference mission provides a context for this thesis that is relevant in light of

the stated goals of the U.S. space program. Conveniently, within the confines of the parking orbit approach, small changes in the parameters of the reference mission have little appreciable effect on the performance measures of interest. That is, raising or lowering the parking orbit altitude or the perilune of the transfer orbit, igniting ahead of or behind the perigee of the transfer orbit, or even changing the target altitude will not significantly affect burn time, ΔV, or the final downrange position of the vehicle. This is illustrated in Figures 2-2, 2-3, 2-4, and 2-5. The implication is that small trajectory errors prior to initialization of powered descent are of little consequence to the performance measures of interest.

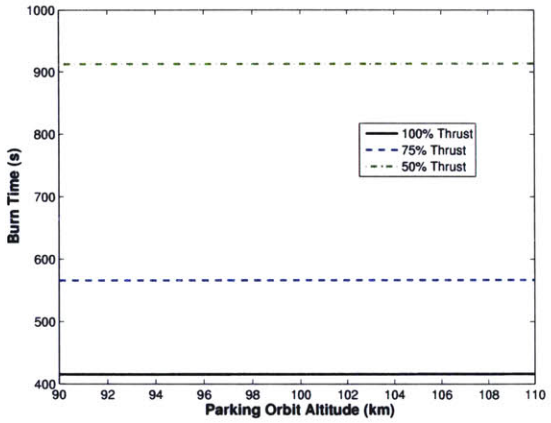

(a) Braking phase duration (burn time)

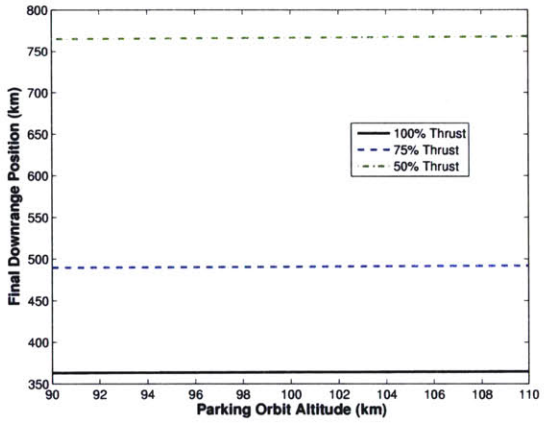

(b) Final downrange position

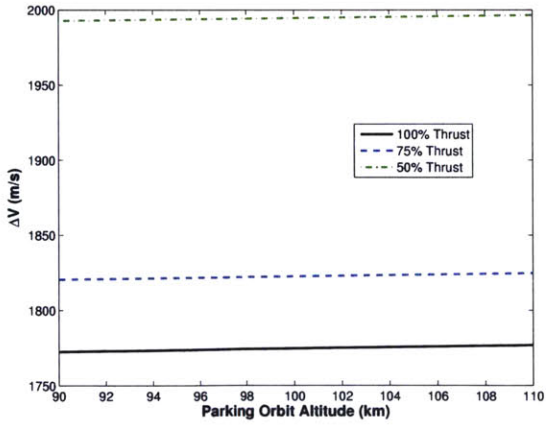

(c) Braking phase ΔV requirement

Figure 2-2: Performance measures versus parking orbit altitude

Each of these figures shows burn time, final downrange position, and ΔV to be

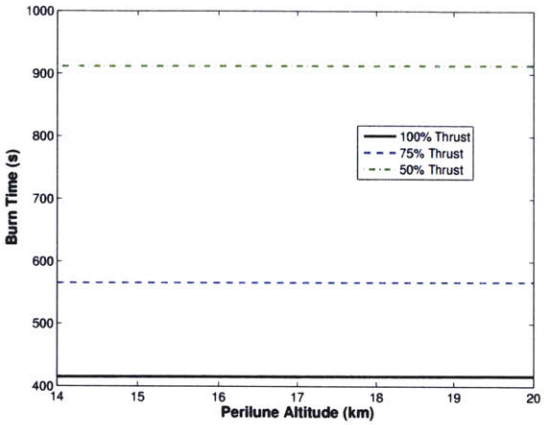

(a) Braking phase duration (burn time)

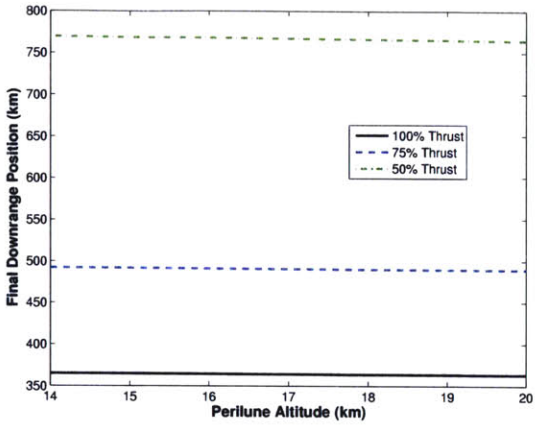

(b) Final downrange position

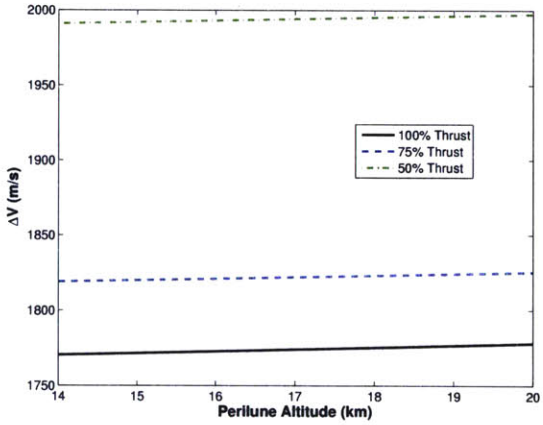

(c) Braking phase ΔV requirement

Figure 2-3: Performance measures versus transfer orbit perilune altitude

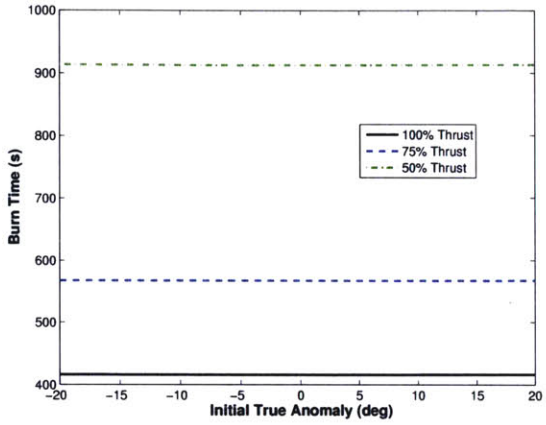

(a) Braking phase duration (burn time)

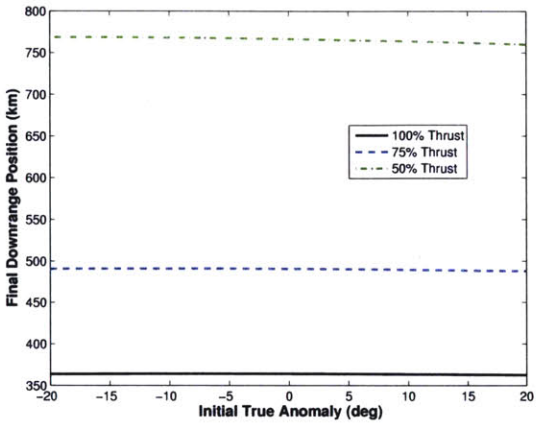

(b) Final Downrange Position

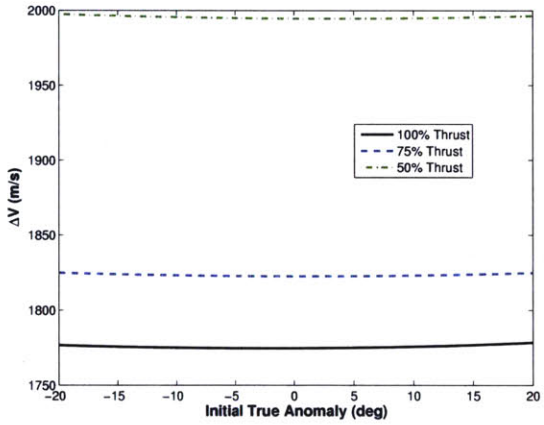

(c) Braking phase ΔV requirement

Figure 2-4: Performance measures versus true anomaly at ignition

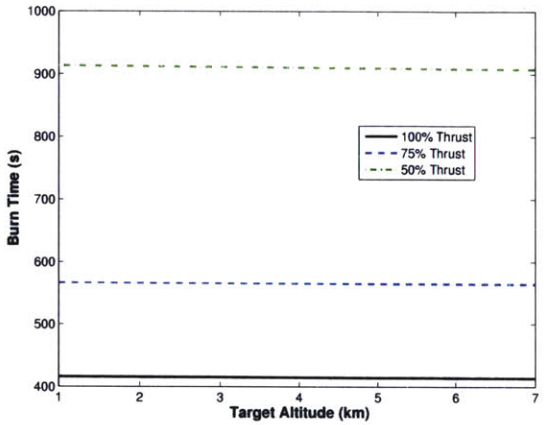

(a) Braking phase duration (burn time)

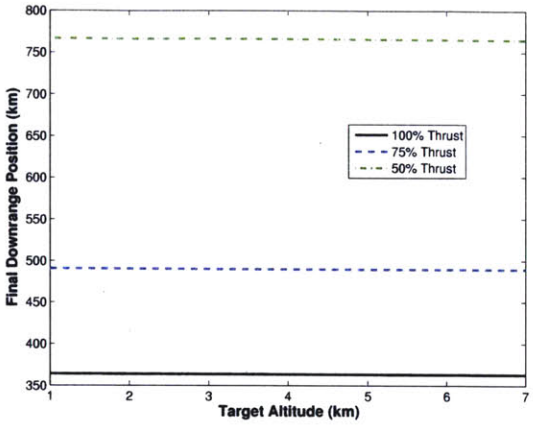

(b) Final downrange position

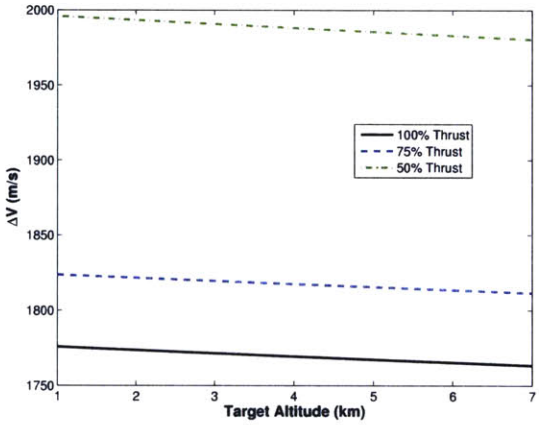

(c) Braking phase ΔV requirement

Figure 2-5: Performance measures versus target altitude

almost flat versus small changes in the reference mission parameters, and the few exceptions are easily explained. For example, Figure 2-2 shows a very slight decrease in the ΔV requirement as parking orbit altitude decreases, which follows since a lower parking orbit altitude would result in a lower velocity at perilune. The ΔV requirement also appears to decrease as the perilune altitude decreases, as shown in Figure 2-3. However, a lower perilune altitude may not be desirable for a descent over a highland region of the Moon. Figure 2-5 shows a marked decrease in the ΔV requirement at higher target altitudes, but if the target altitude were increased, the ΔV requirement for the terminal descent phase would increase as well, offsetting the decrease in the braking phase ΔV. In any case, discussion of the minutiae of Figures 2-2 through 2-5 is tangential to the main point of this section, which is that results obtained assuming the reference mission specified in Table 2.4 will carry over to a variety of missions involving a descent from a lunar parking orbit.

2.3 Performance Characteristics

Since changes to the parameters of the reference mission have little effect on descent performance, the reference mission as defined in Table 2.4 can be assumed throughout this thesis with little bearing on the development and results presented in later chapters. With the reference mission and baseline vehicle specified, it is possible to study the effects of varying a single shutdown time on total burn time, final downrange position, and ΔV requirement. In this section, the 4-engine pair configuration shown in Table 2.3 will be assumed, giving available thrust levels of 100%, 75%, and 50% of maximum thrust.

Figure 2-6 shows three planar, PEG-guided descent trajectories. The horizontal line indicates the target altitude of 1.5 km. The solid trajectory is the nominal full-thrust trajectory, where the vehicle maintains maximum thrust throughout the burn. The dashed and dash-dot trajectories were both flown at maximum thrust for 300 s and at the 75% thrust level from then on. On the dashed trajectory, the shutdown was not anticipated within PEG, while on the dash-dot trajectory, it was.

Hence, the dashed trajectory follows the full-thrust trajectory until it branches off at $t = 300\ s$, while the dash-dot trajectory follows a smooth, lofted arc. It should be noted that the final downrange positions of the two shutdown trajectories are not quite equal. When the shutdown is anticipated, the final downrange position is slightly less than when the shutdown is not anticipated. The fact that there are two types of shutdown trajectories is important in the next chapter, but the slight difference in final downrange position is not.

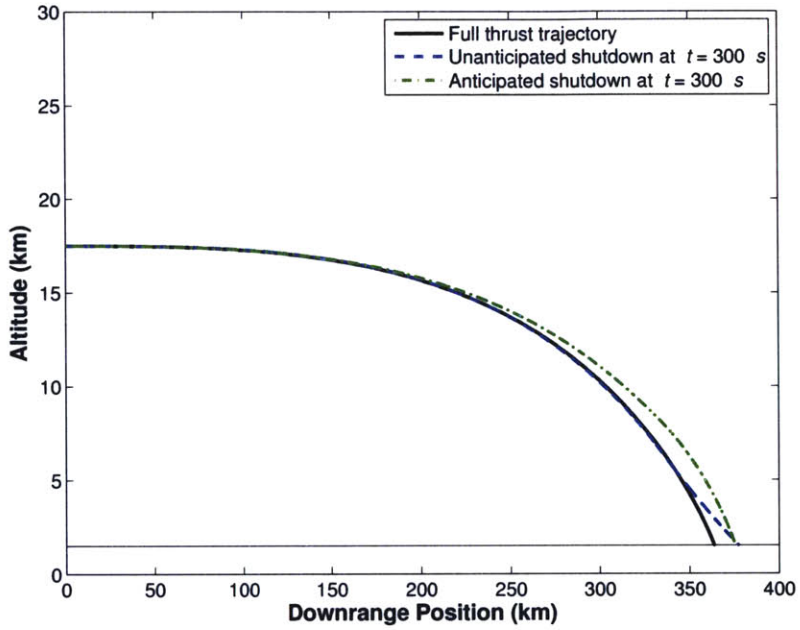

Figure 2-6: Sequential engine shutdown trajectories

Figure 2-7 shows how burn time varies as a function of shutdown time from ignition as the vehicle descends along the full-thrust trajectory of Figure 2-6. Specifically, Figure 2-7 gives the total burn time that results from a transition to some lower thrust level at any time along the descent trajectory. The three available thrust levels are captured in the figure: maximum thrust by the solid line, 75% of the maximum thrust by the dashed line, and 50% of the maximum thrust by the dash-dot line; the earlier the shutdown time, the longer the total burn time. For example, as the dotted line highlights, a total burn time of just under 600 s results from a transition from 100% to 50% of maximum thrust at $t = 300\ s$.

In a similar way, Figure 2-8 shows how the final downrange position varies as a

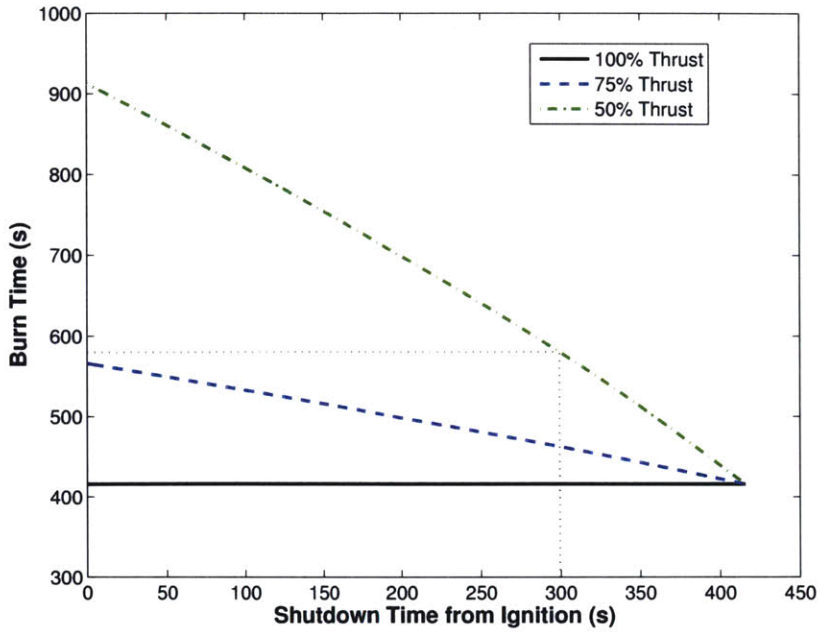

Figure 2-7: Burn time versus shutdown time from ignition

function of shutdown time from ignition along the full-thrust trajectory in Figure 2-6. The dotted line indicates that the final downrange position resulting from a transition from 100% to 50% of maximum thrust at $t = 300\ s$ is just over 400 km, approximately 40 km longer than the final downrange position of the full-thrust trajectory. The distance parallel to the final downrange position axis between the solid and dash-dot lines of Figure 2-8 will be referred to as *coverage*. If the dashed trajectory in Figure 2-6 involved a transition to 50% of maximum thrust rather than 75%, the coverage value at $t = 300\ s$ in Figure 2-8 would correspond to the distance along the target altitude line between the solid and dashed trajectories in Figure 2-6. In general, coverage decreases with time along a descent trajectory and increases as the interval between the maximum and minimum available thrust levels grows.

Finally, Figure 2-9 shows how the ΔV requirement varies as a function of shutdown time from ignition along the full-thrust trajectory of Figure 2-6. As in the previous two figures, the dotted line indicates that a transition from 100% to 50% of maximum thrust at $t = 300\ s$ requires a total ΔV of just over 1,900 m/s, compared to a ΔV of approximately 1,780 m/s when no shutdown occurs.

Figures 2-7, 2-8, and 2-9 are valid as long as the vehicle is on the full-thrust

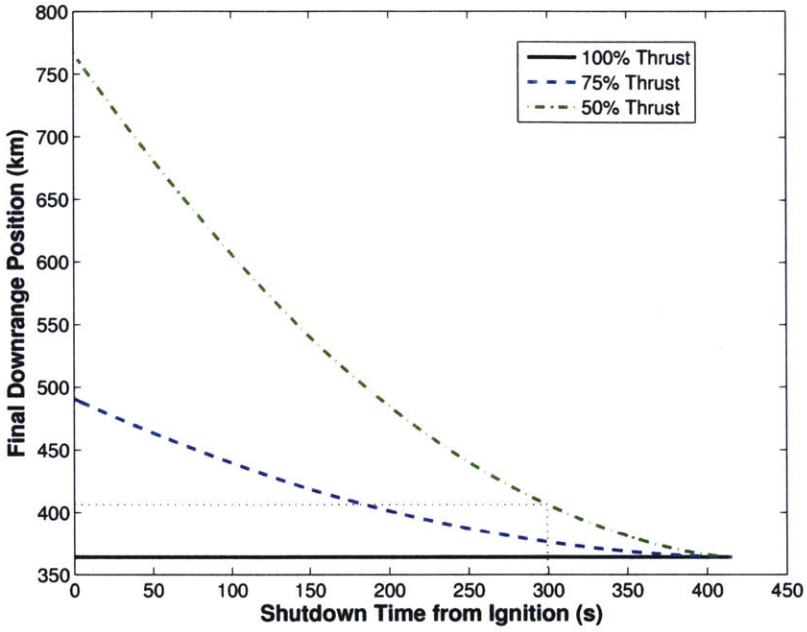

Figure 2-8: Final downrange position versus shutdown time from ignition

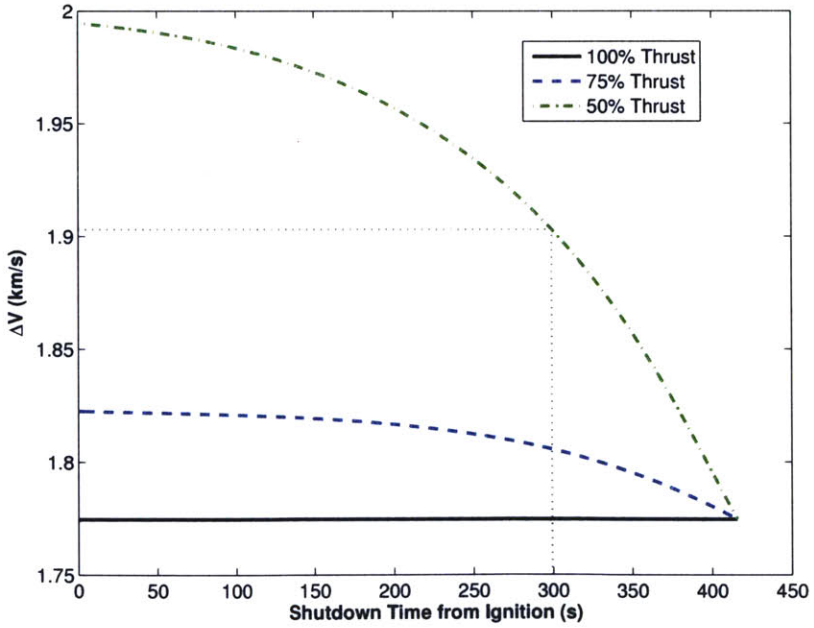

Figure 2-9: ΔV requirement versus shutdown time from ignition

trajectory of Figure 2-6. The 100% thrust trendline is constant (horizontal) in each figure, representing the smallest burn time, shortest final downrange position, and minimum ΔV requirement possible, respectively. It is important to understand how the trendlines evolve once a shutdown has taken place on a vehicle with more than one shutdown available. A notional example is shown in Figure 2-10. The vehicle in this case has three available thrust levels; one shutdown takes place at a time t_{sd_1} from ignition, and the second takes place at time t_{sd_2}. After the first shutdown, the uprange coverage limit, represented by the dark solid line, becomes the value of the coverage trendline corresponding to F_2 at the time of the first shutdown. The downrange coverage limit, represented by the dash-dot line, remains the same at time t_{sd_1}, but the coverage trendline corresponding to F_3 subsequently shallows so that it meets the new uprange coverage limit at the new minimum burn time t_{m_1}. Following the second shutdown at time t_{sd_2}, the final downrange position is fixed. The lighter solid lines show the coverage had the shutdowns not taken place. These lines intersect at t_{m_0}, the minimum burn time with no shutdowns, or at t_{m_1}, the minimum burn time once the first shutdown has taken place.

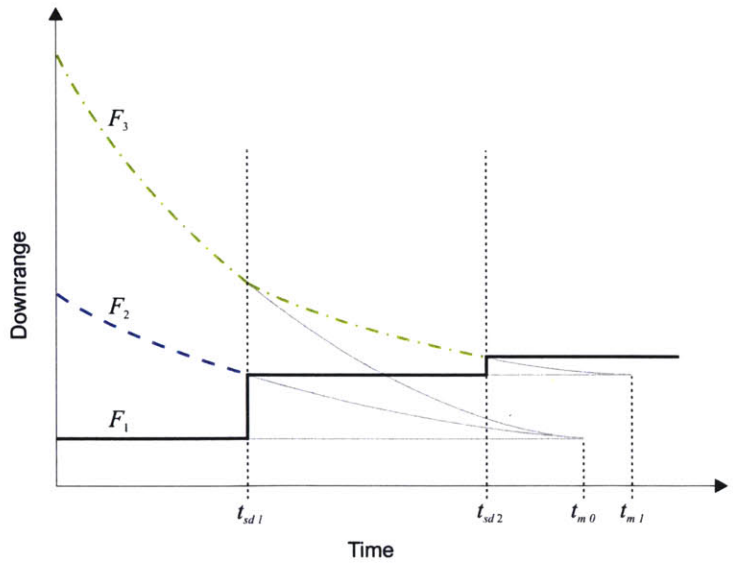

Figure 2-10: Coverage shifts due to shutdowns

Clearly, one effect of a shutdown is an immediate loss of uprange coverage. The other effect is a reduction in the rate of downrange coverage loss as the burn continues.

On the other hand, preserving uprange coverage by not shutting down means that downrange coverage is lost more quickly than it would have been had a shutdown taken place. The shutdown algorithm developed in the next chapter must select the shutdown times in order to maintain the coverage in such a way that the probability of achieving the desired final downrange position is maximized.

It is plausible, though perhaps unlikely, that a vehicle might need to accomodate out-of-plane targets. While a plane change is accomplished most efficiently prior to the initialization of powered descent, it can nevertheless be achieved during the braking phase. PEG can be used to guide a plane change, and shutdowns can be used to control the final downrange position in the new orbital plane. Figure 2-11 shows the terminal braking phase positions possible assuming the baseline vehicle configuration and inclination changes commanded at the outset of the braking phase. Since the term *downrange* refers to the downrange direction at the terminus of the braking phase, the term *down-track* is used in Figure 2-11 to denote the direction of the vehicle velocity in the plane of the transfer orbit projected onto the surface of the Moon.

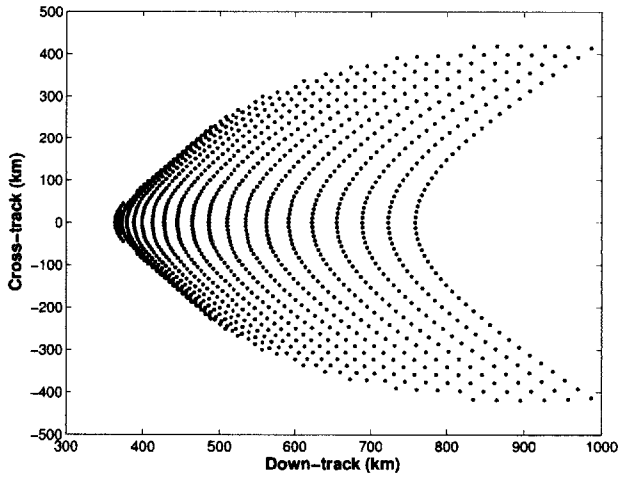

Figure 2-11: Reachable targets using plane changes

Along lines of constant inclination in Figure 2-11, longer final downrange positions correspond to earlier shutdown times. The down-track component of the final position must increase above its nominal value in order change the orbital plane, since the

descent trajectory will shallow as some thrust is directed to effect the plane change. Lines of constant shutdown time, interestingly, resemble hyperbolas in Figure 2-11. Although Figure 2-11 assumes inclination changes commanded at the outset of the braking phase, such changes can be commanded at any time during the descent. However, coverage in the cross-track direction is approximately proportional to coverage in the down-track direction, and thus decays throughout the descent in the manner illustrated in Figure 2-8. It should be noted that trajectories resulting in large lateral offsets from the nominal target position impose substantially higher ΔV requirements than do in-plane trajectories.

A final remark in this section concerns fuel efficiency and sequential engine shutdown. For a PEG-guided descent to some specified terminal position and velocity, fuel efficiency is maximized by maintaining the constant thrust level F_t that allows the terminal conditions to be satisfied. If only a set number discrete thrust levels are available, the most fuel-efficient thrust profile involves a shutdown from the nearest thrust level above F_t to the nearest thrust level below F_t. This is demonstrated analytically in Ref. [16].

2.4 Performance Sensitivity

While small variations in the parameters of the reference mission do not appreciably affect the key vehicle performance characteristics over the powered descent, the same cannot be said for changes to the baseline vehicle definition. Specifically, while the basic relationships between the key performance characteristics and shutdown timing are unaffected, changes to the initial thrust-to-weight ratio or the specific impulse of the vehicle do affect the magnitudes of those characteristics. Examination of the effects of changes to the baseline vehicle definition illustrates the potential impact of off-nominal vehicle performance (e.g., higher or lower than expected thrust).

Figures 2-12 and 2-13 illustrate the effects of decreasing or increasing the initial thrust-to-weight ratio, respectively. The bold foreground lines show burn time, final downrange position, and ΔV as functions of shutdown time for the initial thrust-to-

weight ratios indicated in the captions. The thinner background lines simply replicate the content of Figures 2-7, 2-8, and 2-9 to provide a reference. In Figure 2-12, it can be seen that, with all else constant, decreasing the initial thrust-to-weight ratio (from 3.5 to 3 N/kg) increases burn time and final downrange position, as well as the ΔV requirement.

In line with the expected trend, Figure 2-13 shows a decrease in burn time, final downrange position, and ΔV as the initial thrust-to-weight ratio is increased (from 3.5 to 4 N/kg). It can also be observed that as the initial thrust-to-weight ratio is increased, the trendlines appear more "compressed". The 100% thrust trendlines and the 50% thrust trendlines are closer together in Figure 2-12 than in Figure 2-13. This implies that a lower initial thrust-to-weight ratio results in greater coverage later in the burn, an interesting phenomenon. Although higher thrust is more efficient in terms of ΔV, increasing the initial thrust-to-weight ratio adversely affects coverage.

The effects of changes in specific impulse are somewhat less pronounced, but nonetheless present. Since the baseline vehicle assumes essentially the highest achievable specific impulse, only the effects of decreasing the specific impulse from the baseline value are considered here. Therefore, Figures 2-14 and 2-15 illustrate the same effects. These two figures show decreases in burn time, final downrange position, and ΔV required with decreases in specific impulse. This is counter-intuitive, since specific impulse is a measure of engine efficiency; the higher the specific impulse, the lower the ΔV requirement.

The ΔV over a constant thrust burn is given by the equation

$$\Delta V = \int_0^{t_{go}} \frac{F}{m_0 - \dot{m}t}\, dt \tag{2.3}$$

where $\dot{m} = F/v_{ex}$. Clearly, with thrust and initial mass held constant, a lower specific impulse will yield a higher mass flow rate and a higher level of acceleration later in the burn. The result is a lower net ΔV because although the burn is less efficient, it is also shorter, and the effect of the reduced duration trumps the inefficiency introduced by the decrease in specific impulse. This explains the effect illustrated in Figures 2-

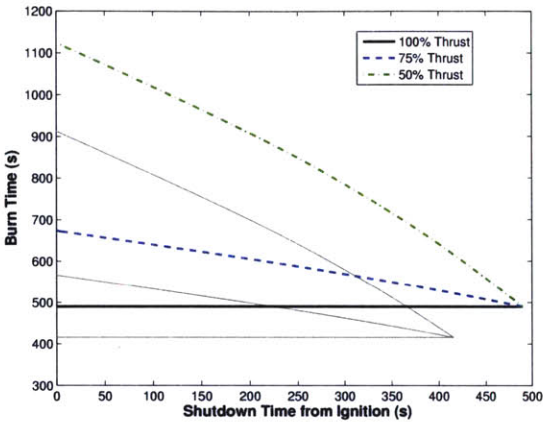

(a) Braking phase duration (burn time)

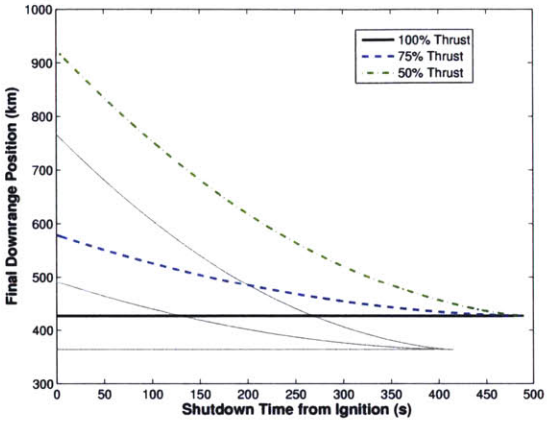

(b) Final downrange position

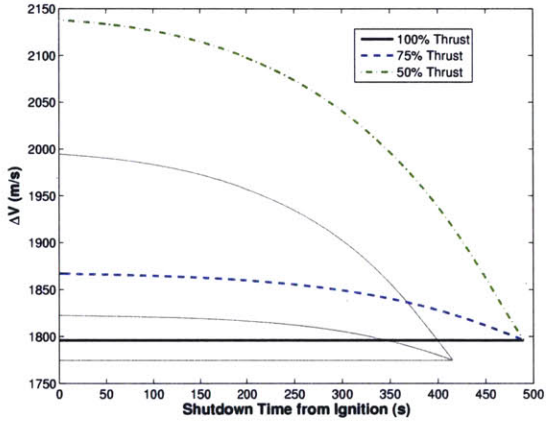

(c) Braking phase ΔV requirement

Figure 2-12: Decreasing the initial thrust-to-weight ratio from 3.5 to 3 N/kg

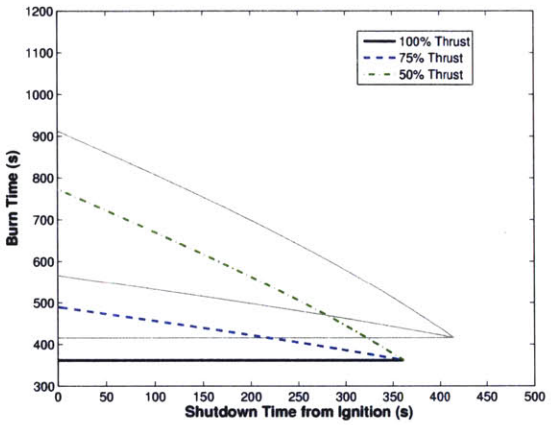

(a) Braking phase duration (burn time)

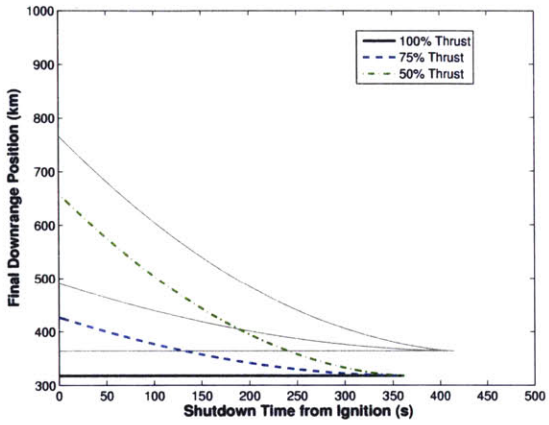

(b) Final downrange position

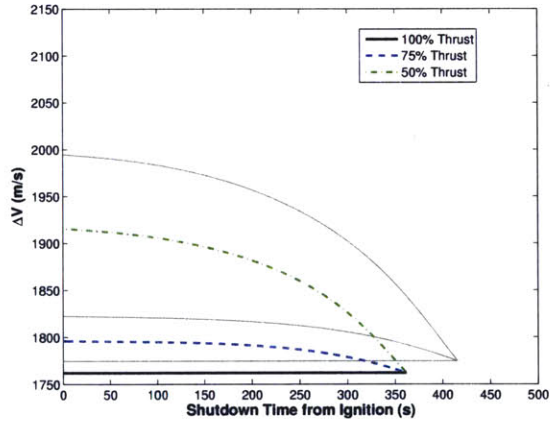

(c) Braking phase ΔV requirement

Figure 2-13: Increasing the initial thrust-to-weight ratio from 3.5 to 4 N/kg

14(c) and 2-15(c), since those figures were generated with the initial thrust-to-weight ratio and initial mass held at their baseline values.

Figures 2-14 and 2-15 are most useful in indicating the potential effects of off-nominal specific impulse performance on burn time, final downrange position, and ΔV. They do not properly capture the effects of a decrease in specific impulse due to a change in the vehicle design. Analyzing the effects of a design change would involve recalculating the initial mass based on the modified specific impulse value. Since no assumption is made in this thesis regarding the mass breakdown of the baseline vehicle, such a calculation cannot be performed, so Figures 2-14 and 2-15 are presented as shown. While burn time, final downrange position, and ΔV are affected by changes in specific impulse, the basic relationship between those performance characteristics and shutdown timing is unaffected. Therefore, since the guidance strategy outlined in the next chapter depends primarily on the fundamental relationship between shutdown timing and final downrange position, it is applicable to a broad range of vehicle designs, not just the vehicle definition employed in this thesis.

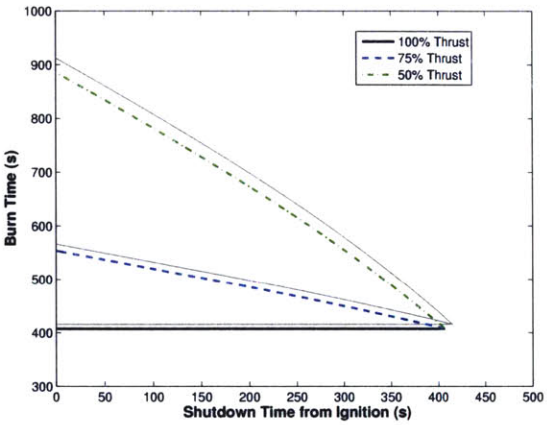

(a) Braking phase duration (burn time)

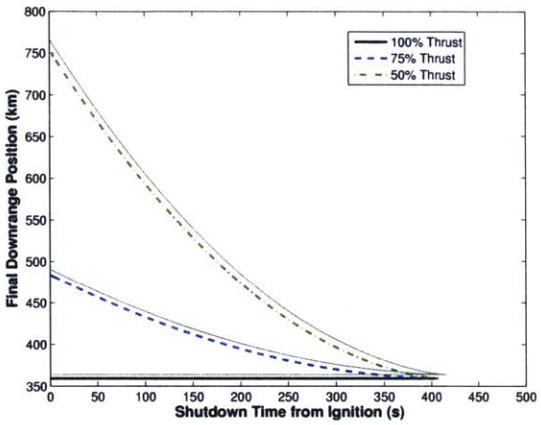

(b) Final downrange position

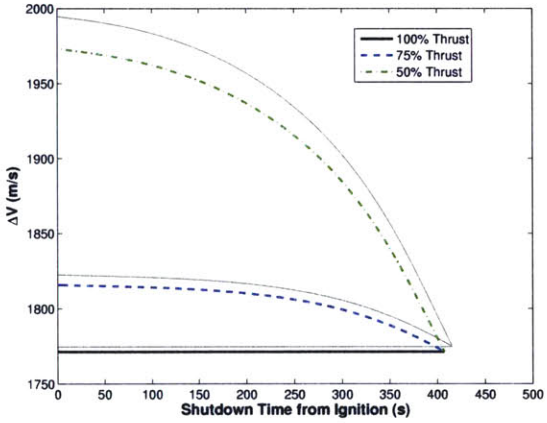

(c) Braking phase ΔV requirement

Figure 2-14: Effects of a decrease in specific impulse, $I_{sp} = 400\ s$

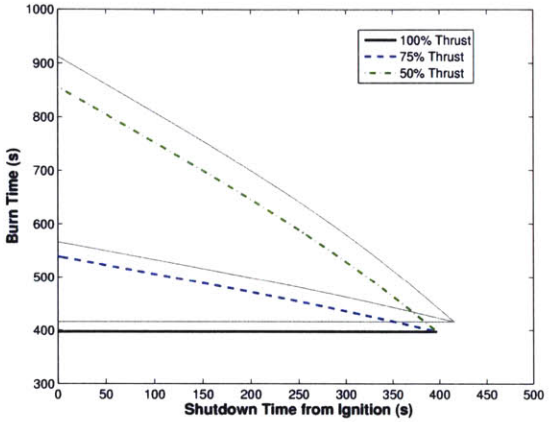

(a) Braking phase duration (burn time)

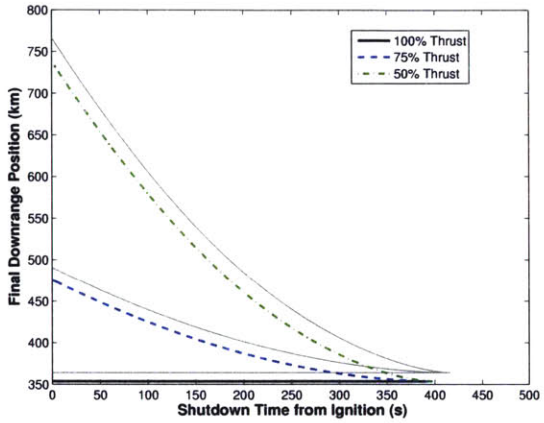

(b) Final downrange position

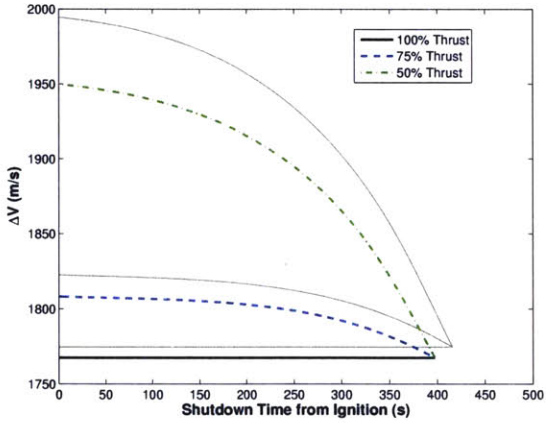

(c) Braking phase ΔV requirement

Figure 2-15: Effects of a decrease in specific impulse, $I_{sp} = 360\ s$

Chapter 3

Guidance Strategy

Having established the performance characteristics of sequential engine shutdown and concluded that their tendencies are more or less insensitive to the vehicle definition and the parameters of the reference mission, it is now possible to develop a guidance strategy wherein control of the final downrange position is provided by selective engine shutdowns. Development proceeds in this chapter in a bottom-up fashion from the perspective of Figure 1-4, which is reproduced below as Figure 3-1. First, the basic PEG equations are derived using the solution to the classic minimum-time orbit injection problem. The application of PEG as a predictor is discussed, since this comes into play in the shutdown algorithm. A throttle computation is introduced that extends the PEG algorithm to allow full control of the final position, and it is shown that a shutdown time computation can be made to provide the same control.

A shutdown algorithm is then developed based on the sequential engine shutdown performance characteristics described in Chapter 2. The basic idea behind the shutdown algorithm is to bias the ignition point uprange and subsequently execute shutdowns, taking into account navigation and vehicle performance uncertainties, such that the desired final downrange position is achieved. A discussion of the details of the shutdown algorithm and its implementation leads into the simulation results presented in Chapter 4.

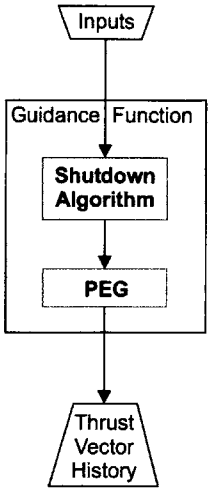

Figure 3-1: Sequential engine shutdown guidance scheme block diagram

3.1 Powered Explicit Guidance

The Powered Explicit Guidance (PEG) algorithm came about in the 1970's as part of the Space Shuttle program. It was originally developed as an ascent guidance algorithm and was subsequently augmented for application to a variety of exoatmospheric maneuvers. The details of PEG appear in a 1979 paper [23] from which this section draws heavily. The strength of PEG lies in its speed and simplicity, which resulted in part from the need to minimize the computational burden imposed by the guidance function.

PEG is based on the solution to the minimum-time orbit injection problem for a flat Earth with uniform gravity and no atmosphere. Consider a vehicle of mass m, acted upon by a thrust force of magnitude F. The vehicle is to be transferred to an altitude h, arriving with velocity $\mathbf{v}_d$ in the least time, as diagrammed in Figure 3-2. The final downrange position is unimportant. The problem is to find the thrust direction angle $\beta(t)$ that will minimize the transfer time. If the vehicle's thrust acceleration history $a(t)$ is known *a priori*, minimizing the transfer time minimizes fuel consumption.

The optimal control law is a bilinear tangent law [24], which has the form

$$\tan\beta = \frac{c_1 + c_2 t}{c_3 + c_4 t} \tag{3.1}$$

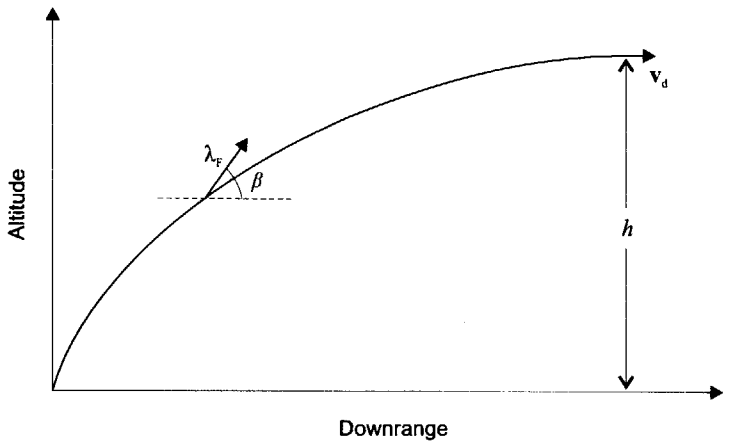

Figure 3-2: Minimum-time orbit injection problem

where c_1, c_2, c_3, and c_4 are constants. In the absence of a terminal constraint on downrange position, $c_4 = 0$, and the optimal control law reduces to a linear tangent law:

$$\tan\beta = \frac{c_1 + c_2 t}{c_3} \tag{3.2}$$

It is not easy to automate the process of solving for the parameters of the bilinear tangent law for a wide variety of maneuvers. Furthermore, in general, the flat Earth assumption does not apply and thus an optimal control law may not exist in closed form. Therein lies the need for a guidance algorithm that closely approximates the optimal control law for the minimum-time orbit injection problem with a formulation that can be extended beyond the flat Earth assumption and is acceptable from a computational standpoint.

As an aside, the distinction between the *linear* and *bilinear* tangent laws can be a source of confusion, but is really just a matter of semantics. In either case, the tip of the thrust direction vector traces a straight-line locus. Bryson [24] makes a distinction between the linear and bilinear tangent laws based upon the coordinate systems to which they are referred. On the right hand sides of Equations (3.1) and (3.2), the numerators and denominators are the altitude and downrange components of the thrust direction vector λ_F, respectively. The locus of thrust direction vectors under a *linear* tangent law would thus be aligned with the vertical axis in the coordinate

system of Figure 3-2, since the downrange component of the thrust direction vector is constant. Under a *bilinear* tangent law, the locus of thrust direction vectors could follow any straight line of non-zero slope. Figure 3-3 illustrates linear and bilinear tangent laws referred to the same coordinate system, with the dashed lines indicating the loci of thrust direction vectors and T denoting the burn cutoff time. The statement that PEG is based on the *bilinear* tangent law refers to an inertial coordinate system, where the locus of thrust direction vectors is not necessarily aligned with one of the three axes. However, as will be shown in the next section, there is a coordinate system in which the PEG steering law is a linear tangent law.

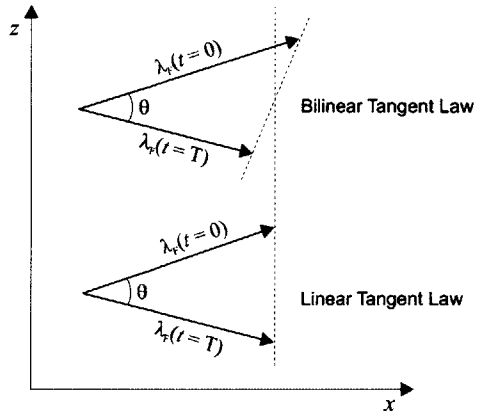

Figure 3-3: Linear and bilinear tangent laws

3.1.1 PEG Equations

Again, consider a vehicle on an ascent trajectory acted upon by a thrust force of magnitude F. As before, the vehicle is to arrive at an altitude h with velocity $\mathbf{v}_d$ in the least time. The objective now is to develop a relatively simple set of equations that yields a good closed form approximation to the optimal thrust direction profile. The vehicle equation of motion is

$$\ddot{\mathbf{r}} = \frac{F}{m}\hat{\lambda}_F + \mathbf{g} \tag{3.3}$$

where $\hat{\lambda}_F$ is a unit vector in the direction of thrust and $\mathbf{g}$ is the gravitational acceleration vector.

A flat Earth is not assumed. However, under the premise that the bilinear tangent law will be near-optimal with repect to fuel consumption absent that assumption, the thrust direction profile is constrained to the form

$$\lambda_F = \lambda + \dot{\lambda}(t - K) \tag{3.4}$$

where λ is a vector in the direction of the velocity-to-be-gained, $\dot{\lambda}$ is a vector representing the rate of change of λ_F, and K is an arbitrary reference time; λ, $\dot{\lambda}$, and K are all constant. Equation (3.4) is a bilinear tangent law in inertial coordinates. To confirm this, the z- and x-components (i.e., altitude and downrange components) of Equation (3.4) can be written separately:

$$\lambda_{F_z} = \lambda_z + \dot{\lambda}_z(t - K)$$

$$\lambda_{F_x} = \lambda_x + \dot{\lambda}_x(t - K)$$

Dividing the z-component by the x-component yields

$$\tan\beta = \frac{\lambda_z + \dot{\lambda}_z(t - K)}{\lambda_x + \dot{\lambda}_x(t - K)} \tag{3.5}$$

Equation (3.5) is identical to Equation (3.1), with $c_1 = \lambda_z - K\dot{\lambda}_z$, $c_2 = \dot{\lambda}_z$, $c_3 = \lambda_x - K\dot{\lambda}_x$, and $c_4 = \dot{\lambda}_x$. Figure 3-4 illustrates the geometry of λ_F, λ and $\dot{\lambda}$; t_{go} is the remaining burn time. Inspection of Figure 3-4 reveals that for a given $\dot{\lambda}$, there are multiple sets of λ and K that give the same time history of λ_F.

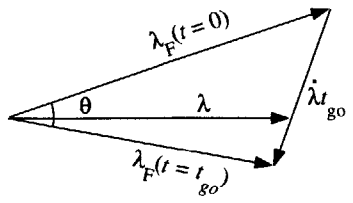

Figure 3-4: Geometry of λ_F, λ and $\dot{\lambda}$ in a bilinear tangent law

In the vehicle equation of motion (3.3), λ_F appears as a unit vector, i.e., only its direction is important. Therefore, Equation (3.4) can be scaled arbitrarily, since changes in the magnitude of λ_F will have no effect on its direction. Equation (3.4) is scaled such that the first term on the right hand side is a unit vector:

$$\lambda_F = \hat{\lambda} + \dot{\lambda}(t - K) \tag{3.6}$$

The convenience of this particular scaling will become apparent later.

When the thrust arc – denoted by θ in Figure 3-4 – is sufficiently small, the magnitude of λ_F remains close to one over the duration of the burn.* Therefore, the unit thrust direction vector is approximated by Equation (3.6):

$$\hat{\lambda}_F \approx \hat{\lambda} + \dot{\lambda}(t - K) \tag{3.7}$$

Substituting Equation (3.7) into Equation (3.3) and rearranging yields the following *approximate* form of the vehicle equation of motion:

$$\ddot{\mathbf{r}} - \mathbf{g} = \frac{F}{m}[\hat{\lambda} + \dot{\lambda}(t - K)] \tag{3.8}$$

It must be assumed that t_{go} is known or has been estimated, because it is never explicitly solved for in this section. Before integrating Equation (3.8), four scalar integrals and two vector integrals are defined, with s denoting a dummy variable of integration:

$$L = \int_0^{t_{go}} \frac{F}{m}\, dt \tag{3.9}$$

$$J = \int_0^{t_{go}} \frac{F}{m}\, t\, dt \tag{3.10}$$

*The implication is that $\dot{\lambda} t_{go}$ is small if θ is small. Under a bilinear tangent law, this is not necessarily true. For example, the locus of thrust direction vectors in Figure 3-4 could be nearly horizontal. However, under a constraint on the angle between $\hat{\lambda}$ and $\dot{\lambda}$ introduced later in this section, it will become possible to make λ_F arbitrarily close to one over the duration of the burn by making θ sufficiently small.

$$S = \int_0^{t_{go}} \int_0^t \frac{F}{m}\, ds\, dt \tag{3.11}$$

$$Q = \int_0^{t_{go}} \int_0^t \frac{F}{m}\, s\, ds\, dt \tag{3.12}$$

$$\mathbf{v}_{grav} = \int_0^{t_{go}} \mathbf{g}\, dt \tag{3.13}$$

$$\mathbf{r}_{grav} = \int_0^{t_{go}} \int_0^t \mathbf{g}\, ds\, dt \tag{3.14}$$

Evaluation of the integrals in Equations (3.9–3.14) is left to the next section. Integrating Equation (3.8) over the remaining burn time, using the definitions in Equations (3.9–3.14), yields

$$\mathbf{v}_d - \mathbf{v} - \mathbf{v}_{grav} = L\hat{\lambda} + (J - KL)\dot{\lambda} \tag{3.15}$$

Integrating a second time yields

$$\mathbf{r}_d - \mathbf{r} - \mathbf{v}t_{go} - \mathbf{r}_{grav} = S\hat{\lambda} + (Q - KS)\dot{\lambda} \tag{3.16}$$

Equations (3.15) and (3.16) include the terminal constraints on the minimum-time orbit injection problem. The desired terminal velocity $\mathbf{v}_d$ appears explicitly in Equation (3.15), and the desired terminal altitude is implicit in the desired terminal position $\mathbf{r}_d$ in Equation (3.16). The vectors $\mathbf{v}_{go}$ and $\mathbf{r}_{go}$ are defined to be the velocity and position-to-be-gained by thrust, i.e., the left-hand sides of Equations (3.15) and (3.16), respectively. Those equations can then be written as

$$\mathbf{v}_{go} = L\hat{\lambda} + (J - KL)\dot{\lambda} \tag{3.17}$$

$$\mathbf{r}_{go} = S\hat{\lambda} + (Q - KS)\dot{\lambda} \tag{3.18}$$

Equations (3.17) and (3.18) provide five scalar equations in seven unknowns. The scalar equations number five rather than six because the downrange component of the desired terminal position is unspecified. The scaling of Equation (3.4) effectively provides a sixth equation. The seven unknowns are the three components each of $\hat{\lambda}$ and $\dot{\lambda}$ and the remaining burn time t_{go}. The problem is therefore underdetermined, and an additional scalar constraint is required for a unique solution to exist. The constraint is chosen to force $\dot{\lambda}$ to be orthogonal to $\hat{\lambda}$:

$$\hat{\lambda} \cdot \dot{\lambda} = 0 \tag{3.19}$$

Under this orthogonality constraint, Equation (3.6) becomes a linear tangent law in the coordinate frame defined by $\hat{\lambda}$ and $\dot{\lambda}$, as illustrated in Figure 3-5. On a nominal Shuttle ascent, the thrust arc is on the order of 45°. Therefore, given Equation (3.19), $1 \leq \lambda_F < 1.1$, which validates the approximation made in Equation (3.7).

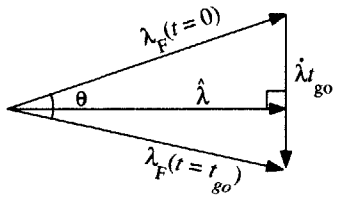

Figure 3-5: Geometry of λ_F, $\hat{\lambda}$, and $\dot{\lambda}$ given Equation (3.19)

Taking the dot product of $\hat{\lambda}$ with Equation (3.17) and substituting Equation (3.19) into the result yields

$$\hat{\lambda} \cdot \mathbf{v}_{go} = L \tag{3.20}$$

Since $\hat{\lambda}$ is a unit vector, $L = |\mathbf{v}_{go}|$, and

$$\hat{\lambda} = \frac{\mathbf{v}_{go}}{v_{go}} \tag{3.21}$$

Taking the dot product of $\hat{\lambda}$ with Equation (3.18) and substituting Equation (3.19) into the result yields

$$\hat{\lambda} \cdot \mathbf{r}_{go} = S \tag{3.22}$$

Earlier, $\mathbf{r}_{go}$ was defined as the left hand side of Equation (3.16). However, the downrange component of $\mathbf{r}_d$ is unspecified. Therefore, the two known components of $\mathbf{r}_{go}$ must be isolated so that Equation (3.22) can be solved for the unknown component. Let $\mathbf{i}_y$ be a unit vector normal to the desired orbital plane, $\mathbf{i}_\xi$ be a unit vector in the radial direction at cutoff (the direction of $\mathbf{r}_d$), and $\mathbf{i}_\zeta$ be a unit vector in the downrange direction at cutoff (i.e., $\mathbf{i}_\zeta = \mathbf{i}_\xi \times \mathbf{i}_y$). Then

$$\mathbf{r}_{go_{\xi y}} = \tilde{\mathbf{r}}_{go} - (\tilde{\mathbf{r}}_{go} \cdot \mathbf{i}_\zeta)\mathbf{i}_\zeta \tag{3.23}$$

$$r_{go_\zeta} = \frac{S - \hat{\lambda} \cdot \mathbf{r}_{go_{\xi y}}}{\hat{\lambda} \cdot \mathbf{i}_\zeta} \tag{3.24}$$

$$\mathbf{r}_{go} = \mathbf{r}_{go_{xy}} + r_{go_\zeta}\mathbf{i}_\zeta \,. \tag{3.25}$$

In Equation (3.23), the tilde over $\mathbf{r}_{go}$ denotes that the downrange component is unspecified. With $\mathbf{r}_{go}$ completely defined, Equation (3.18) can be solved for $\dot{\lambda}$:

$$\dot{\lambda} = \frac{\mathbf{r}_{go} - S\hat{\lambda}}{Q - KS} \tag{3.26}$$

The reference time K is defined as

$$K = \frac{J}{L} \tag{3.27}$$

This definition ensures that Equation (3.17) is consistent with Equation (3.21).

The equations developed in this section are mechanized using an iterative predictor-corrector formulation with $\mathbf{v}_{go}$ as the independent variable. The choice of $\mathbf{v}_{go}$ as the independent variable gives the most straightforward means of correction. From estimates of $\mathbf{v}_{go}$ and $\mathbf{r}_d$, the basis vectors for the steering law, $\hat{\lambda}$ and $\dot{\lambda}$, and the reference time K are calculated. The basis vectors and reference time are then used to cal-

culate predicted final position and velocity, and the difference between the desired and predicted final velocities is added to $\mathbf{v}_{go}$. If the magnitude of this difference is small compared to the updated v_{go}, PEG is declared converged. Otherwise, a new iteration commences. During a burn, PEG is periodically cycled to recalculate the basis vectors and reference time.

3.1.2 Thrust and Gravity Integrals

Thrust Integrals

If thrust is a constant, the thrust integrals defined in Equations (3.9–3.12) can be integrated in closed form, since an estimate for t_{go} has been assumed. Exhaust velocity is assumed to be constant, and τ is defined as the ratio of exhaust velocity to initial acceleration

$$\tau = \frac{v_{ex}}{F/m_0} \tag{3.28}$$

The resulting expressions are:

$$L = -v_{ex} \ln(1 - \frac{t_{go}}{\tau}) \tag{3.29}$$

$$S = L(t_{go} - \tau) + v_{ex} t_{go} \tag{3.30}$$

$$J = Lt_{go} - S \tag{3.31}$$

$$Q = S\tau - \frac{v_{ex} t_{go}^2}{2} \tag{3.32}$$

Equations (3.29–3.32) are valid for a single-phase burn. For a multiple-phase burn, where the i-th phase has the vehicle operating at some constant thrust F_i over a time interval t_{b_i}, evaluation of the thrust integrals involves an integration loop over the remaining phases. The calculation proceeds as follows, with k denoting the current

phase, N denoting the total number of phases, and the i-th phase transition time specified by t_{sd_i}, the time at which the thrust level switches from F_i to F_{i+1}.

The thrust integrals L, J, S, and Q are initialized to zero. The first step in the loop is the calculation of t_{b_i}. If $i = k$, then

$$t_{b_i} = \min[t_{sd_i} - t,\ \tau_i(1 - e^{-(v_{go}-L)/v_{ex}})] \tag{3.33}$$

Otherwise, $i > k$, and

$$t_{b_i} = \min[t_{sd_i} - t_{sd_{i-1}},\ \tau_i(1 - e^{-(v_{go}-L)/v_{ex}})] \tag{3.34}$$

Next, t_{go_a} is defined as

$$t_{go_a} = \sum_{k}^{i-1} t_{b_j} \tag{3.35}$$

The thrust integrals are then evaluated over thrust phase i. The resulting expressions look somewhat similar to Equations (3.29–3.32).

$$L_i = -v_{ex} \ln(1 - t_{b_i}/\tau_i) \tag{3.36}$$

$$S_i = -(\tau_i - t_{b_i})L + v_{ex}t_{b_i} + Lt_{b_i} \tag{3.37}$$

$$J_i = L_i \sum_{k}^{i} t_{b_j} - S_i \tag{3.38}$$

$$Q_i = S_i(\tau_i + t_{go_a}) - \frac{1}{2}v_{ex}t_{b_i}^2 + Jt_{b_i} \tag{3.39}$$

These quantities are then added into the total thrust integrals over the burn, that is, $L = L + L_i$, $J = J + J_i$, etc. Finally, τ_{i+1} is calculated as

$$\tau_{i+1} = \frac{v_{ex}}{F_{i+1}/m_{i+1}} \tag{3.40}$$

with $m_{i+1} = m_i - \frac{F_i}{v_{ex}} t_{b_i}$. When $i = N$, L_i and t_{b_i} are calculated as

$$L_i = v_{go} - L \tag{3.41}$$

$$t_{b_i} = \tau_i (1 - e^{-L_i / v_{ex}}) \tag{3.42}$$

with the equations for S_i, J_i, and Q_i as given earlier. It should be noted that the exhaust velocity could be different for each phase of the burn, but the above equations take it as constant over the entire burn.

Gravity Integrals

As implemented on the Space Shuttle [23], $\mathbf{v}_{grav}$ and $\mathbf{r}_{grav}$ are approximated within PEG from a coasting trajectory that is close to the powered trajectory. This technique provides an accurate and computationally efficient way to calculate the effects of gravity over a burn. A powered trajectory of the following form is assumed:

$$\mathbf{r}_P = \nu_0 + \nu_1 t + \nu_2 t^2 + \nu_3 t^3 \tag{3.43}$$

$$\mathbf{v}_P = \nu_1 + 2\nu_2 t + 3\nu_3 t^2 \tag{3.44}$$

At $t = 0$, $\mathbf{r}_P = \mathbf{r}$ and $\mathbf{v}_P = \mathbf{v}$, therefore $\nu_0 = \mathbf{r}$ and $\nu_1 = \mathbf{v}$. At $t = t_{go}$,

$$\mathbf{r} + \mathbf{v} t_{go} + \mathbf{r}_{thrust} = \nu_0 + \nu_1 t_{go} + \nu_2 t_{go}^2 + \nu_3 t_{go}^3 \tag{3.45}$$

$$\mathbf{v} + \mathbf{v}_{thrust} = \nu_1 + 2\nu_2 t_{go} + 3\nu_3 t_{go}^2 \tag{3.46}$$

Equations (3.45) and (3.46) can be solved for ν_2 and ν_3, yielding

$$\nu_2 = \frac{3\mathbf{r}_{thrust} - \mathbf{v}_{thrust} t_{go}}{t_{go}^2} \tag{3.47}$$

$$\nu_3 = \frac{-2\mathbf{r}_{thrust} + \mathbf{v}_{thrust} t_{go}}{t_{go}^3} \tag{3.48}$$

A coasting trajectory of the following form is assumed:

$$\mathbf{r}_c = \nu_0' + \nu_1' t \tag{3.49}$$

$$\mathbf{v}_c = \nu_1' \tag{3.50}$$

The coefficients ν_0' and ν_1' are chosen to satisfy the following two conditions:

$$\int_0^{t_{go}} [\mathbf{r}_c(t) - \mathbf{r}_P(t)]\, dt = 0 \tag{3.51}$$

$$\int_0^{t_{go}} [\mathbf{r}_c(t) - \mathbf{r}_P(t)]\, (t_{go} - t)\, dt = 0 \tag{3.52}$$

Equation (3.52) weights earlier differences between the powered and coasting trajectories more heavily than later differences. Solving Equations (3.51) and (3.52) for ν_0' and ν_1', the initial position and velocity on the coasting trajectory, yields

$$\nu_0' = \mathbf{r} - \frac{1}{10}\mathbf{r}_{thrust} - \frac{1}{30}\mathbf{v}_{thrust} t_{go} = \mathbf{r}_{c_1} \tag{3.53}$$

$$\nu_1' = \mathbf{v} + \frac{6}{5}\mathbf{r}_{thrust}/t_{go} - \frac{1}{10}\mathbf{v}_{thrust} = \mathbf{v}_{c_1} \tag{3.54}$$

Numerical integration or an analytical conic state propagation routine can be used to extrapolate $\mathbf{r}_c$ and $\mathbf{v}_c$ through the burn time t_{go} to obtain $\mathbf{r}_{c_2}$ and $\mathbf{v}_{c_2}$. The vectors $\mathbf{v}_{grav}$ and $\mathbf{r}_{grav}$ are then given by

$$\mathbf{v}_{grav} = \mathbf{v}_{c_2} - \mathbf{v}_{c_1} \tag{3.55}$$

$$\mathbf{r}_{grav} = \mathbf{r}_{c_2} - \mathbf{r}_{c_1} - \mathbf{v}_{c_1} t_{go} \tag{3.56}$$

3.1.3 Prediction Using PEG

The PEG algorithm is extremely useful as a prediction tool, because the predictor-corrector formulation necessarily involves calculating the predicted final position and velocity at the end of the burn without numerically integrating the vehicle equation of motion. The predicted position and velocity can be written as

$$\mathbf{v}_p = \mathbf{v} + \mathbf{v}_{thrust} + \mathbf{v}_{grav} \tag{3.57}$$

$$\mathbf{r}_p = \mathbf{r} + \mathbf{v}t_{go} + \mathbf{r}_{thrust} + \mathbf{r}_{grav} \tag{3.58}$$

with $\mathbf{v}_{grav}$ and $\mathbf{r}_{grav}$ as defined in Equations (3.13) and (3.14), and $\mathbf{v}_{thrust}$ and $\mathbf{r}_{thrust}$ defined as

$$\mathbf{v}_{thrust} = \int_0^{t_{go}} \frac{F}{m} \frac{\hat{\lambda} + \dot{\lambda}(t-K)}{|\hat{\lambda} + \dot{\lambda}(t-K)|}\, dt \tag{3.59}$$

$$\mathbf{r}_{thrust} = \int_0^{t_{go}} \int_0^{t} \frac{F}{m} \frac{\hat{\lambda} + \dot{\lambda}(s-K)}{|\hat{\lambda} + \dot{\lambda}(s-K)|}\, ds\, dt \tag{3.60}$$

The quantities $\mathbf{v}_{thrust}$ and $\mathbf{r}_{thrust}$ can be approximated to first order by the right-hand sides of Equations (3.15) and (3.16). However, the inaccuracy of that approximation grows as the thrust arc increases, affecting the convergence of PEG and imposing restrictions on its operating range. There is a better method of evaluating $\mathbf{v}_{thrust}$ and $\mathbf{r}_{thrust}$ which removes these deficiencies and greatly improves the accuracy of PEG predictions.

The actual thrust acceleration profile can be accurately approximated by a quadratic polynomial. If a thrust acceleration profile of the form

$$a(t) = A + B(t-K) + C(t-K)^2 \tag{3.61}$$

is substituted for the F/m term in Equations (3.59) and (3.60), the resulting integrals can be evaluated in closed form. Thus, with proper selection of the coefficients A,

B, and C, very accurate estimates of $\mathbf{v}_{thrust}$ and $\mathbf{r}_{thrust}$ can be obtained.[†] Since the turning rate basis vector $\dot{\lambda}$ is calculated from the simplified expression (3.18) for the position-to-be-gained $\mathbf{r}_{go}$, use of any higher order prediction method causes $\mathbf{r}_{go}$ to be inconsistent with $\mathbf{r}_{thrust}$. Thus, a bias term

$$\mathbf{r}_{bias} = \mathbf{r}_{go} - \mathbf{r}_{thrust} \tag{3.62}$$

must be added into the calculation of $\mathbf{r}_{go}$. Of course, $\mathbf{v}_{thrust}$ and $\mathbf{r}_{thrust}$ can be calculated using numerical integration, but with only marginal improvement in accuracy at a relatively high cost in computation.

3.1.4 Final Downrange Position Control

With only the direction of thrust available as a control, the final downrange position of a PEG-guided burn is fixed by the initial and terminal conditions and the thrust acceleration history. A throttleable rocket engine provides the extra degree of freedom needed to control the final downrange position. Generally, the throttle computation is implemented as an outer loop around the predictor-corrector which adjusts the throttle setting to achieve the desired final downrange position, as diagrammed in Figure 3-6. A lower throttle setting results in a greater final downrange position.

On each pass through the throttle computation, the change in thrust needed to null the "range angle" error is calculated.[‡] The range angle is simply the central angle to be traversed over the remaining portion of the burn. The appropriate change in thrust ΔF is related to the range angle error $\Delta\phi = \phi_d - \phi_p$ by

$$\Delta F = \frac{dF}{d\phi}\Delta\phi \tag{3.63}$$

which can be expanded to

[†]This technique was originally developed by Thomas Fill of the Charles Stark Draper Laboratory in 1980.

[‡]The derivation of the throttle computation presented in Section 3.1.4 was adapted with permission from a 1991 memo authored by Gerald Condon of the NASA Johnson Space Center.

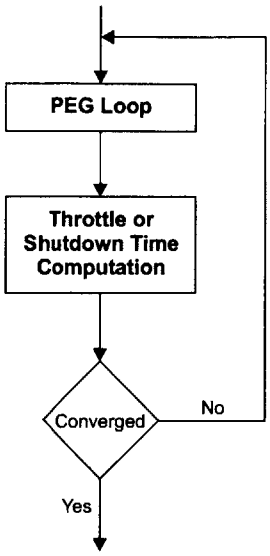

Figure 3-6: Throttle loop block diagram

$$\Delta F = \frac{dF}{dt_{go}} \frac{dt_{go}}{d\phi} \Delta\phi \tag{3.64}$$

The derivative of F with respect to t_{go} can be obtained by differentiating the rocket equation

$$t_{go} = \frac{v_{ex} m}{F} (1 - e^{-v_{go}/v_{ex}}) \tag{3.65}$$

with respect to F, which yields

$$\frac{dt_{go}}{dF} = -\frac{v_{ex} m}{F^2} (1 - e^{-v_{go}/v_{ex}}) \tag{3.66}$$

and inverting this result to get

$$\frac{dF}{dt_{go}} = -\frac{F^2}{v_{ex} m} \frac{1}{(1 - e^{-v_{go}/v_{ex}})} \tag{3.67}$$

The derivative of t_{go} with respect to ϕ can be approximated by recognizing that a change in final downrange position is related to a change in t_{go} by the horizontal component of the current vehicle velocity v_h, namely

$$\Delta r_{dr} \approx v_h \Delta t_{go} \tag{3.68}$$

There is also a relationship between a change in final downrange position and a change in range angle, namely

$$\Delta r_{dr} \approx r \Delta \phi \tag{3.69}$$

where r is the magnitude of the current position vector. Equating the two approximate expressions for Δr_{dr} yields

$$\frac{dt_{go}}{d\phi} = \frac{r}{v_h} \tag{3.70}$$

Substituting Equations (3.67) and (3.70) into Equation (3.64) yields a closed form expression for the change in thrust magnitude required to null the range angle error

$$\Delta F = -\frac{F}{v_{ex} m (1 - e^{-v_{go}/v_{ex}})} \frac{r}{v_h} \Delta \phi \tag{3.71}$$

It can be seen from Equation (3.71) that if the the vehicle is coming down short of its target, $\Delta\phi$ will be positive, and the resulting change in thrust will be negative. If the vehicle is aimed long, $\Delta\phi$ will be negative, and the change in thrust will be positive, hence the earlier assertion that a lower thrust level increases the final downrange position, while a higher thrust level has the opposite effect.

As indicated by the block diagram in Figure 3-6, a single shutdown time calculation can be used in an analogous manner to the throttle computation to null the range angle error. A simple "guess and check" numerical algorithm (e.g., bisection) is sufficient. Convergence can be guaranteed, provided coverage is sufficient, and the initial guess does not have to be particularly good.

3.2 Shutdown Algorithm

Although a single shutdown can, in principle, be used to null downrange position error, it is not clear that just one shutdown is sufficient to contend with uncertainties resulting from imperfect navigation and off-nominal vehicle performance. Therefore, this section develops a heuristic that guides the use of multiple shutdowns. It was illustrated in Section 2.3 that once a shutdown has been executed, some uprange coverage is lost and cannot be recovered. Since navigation and vehicle performance errors have an unpredictable effect on the final downrange position, the ignition point must be biased uprange in order to decrease the likelihood that the vehicle will overshoot the target. The term *shutdown algorithm* refers to the combination of an ignition bias plus a method of calculating shutdown times during the braking phase, such that the desired final downrange position is achieved.

3.2.1 Biasing the Ignition Point

A key part of any descent guidance function, whether or not there is active control of the final downrange position, is the calculation of the position uprange of the target at which the powered descent should be initiated. For example, if the final downrange position is fixed by the thrust acceleration profile and the boundary conditions for the burn, the ignition bias provides the only measure of downrange control, as illustrated in Figure 3-7. The shutdown algorithm calculates the ignition bias such that the likelihood of the vehicle landing downrange of the target is low if maximum thrust is maintained throughout the burn.

The value of the ignition bias is a function of the effects of state estimate errors and off-nominal vehicle performance over the entire braking phase. As such, it is most reliably calculated from a distribution of final downrange position errors generated by Monte Carlo trials of a braking phase simulation in which the vehicle thrust is fixed at its maximum value (see Section 4.2.1). The value of the ignition bias used in the shutdown algorithm, 7.5 km, was calculated as three times the standard deviation of the distribution shown in Figure 4-4.

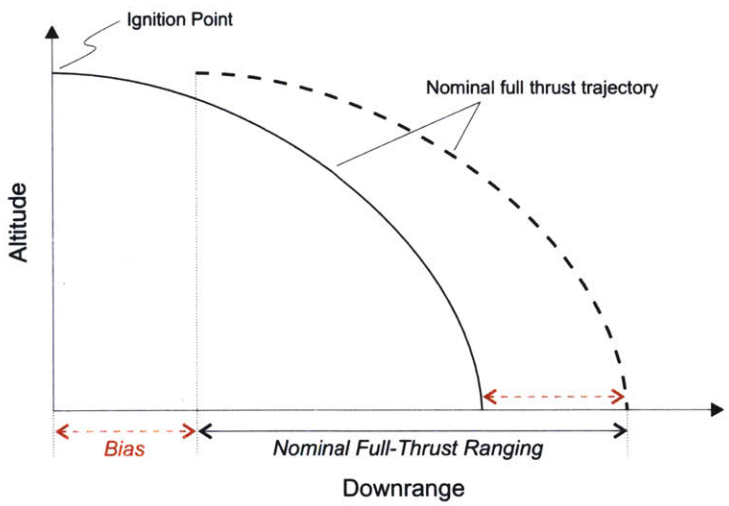

Figure 3-7: Biasing the ignition point

3.2.2 Calculating Shutdown Times

Shutdown times are calculated on the basis of the estimated vehicle state as well as the error covariance that characterizes that estimate. Uncertainties in vehicle performance are also accounted for. In order to describe the method used to select shutdown times, it is necessary to first elaborate on a few concepts illustrated in Figure 3-8. In this section, where subscripts $1, 2, ..., N$ refer to thrust levels, a 1 indicates the highest available thrust level, 2 the next highest, and so forth, with N denoting the lowest available thrust level. A subscript k denotes the current thrust level. The i-th shutdown time t_{sd_i} is the time at which the vehicle transitions from thrust level i to thrust level $(i+1)$.

At any time during the braking burn, the coverage (defined in Section 2.3) provided by each available thrust level can be predicted over the remainder of the burn. The quantity *downrange-to-target*, denoted by D_{go}, refers to the distance along the surface of the Moon between the current vehicle position vector and the target position vector, as shown in Figure 3-8(a), and is described by the expression

$$D_{go} = R_M \cos^{-1}\left(\mathbf{i}_r \cdot \mathbf{i}_{r_T}\right) \tag{3.72}$$

where R_M is the radius of the Moon (which is assumed to be perfectly spherical in

this thesis), $\mathbf{i}_r$ is a unit vector in the direction of the instantaneous vehicle position, and $\mathbf{i}_{r_T}$ is a unit vector in the direction of the target position. The total coverage at any time is bounded by the uprange and downrange *coverage limits*. The uprange coverage limit D_u is the final downrange position that would be reached if the vehicle were to maintain the maximum available thrust setting for the duration of the braking burn. The downrange coverage limit D_d is the final downrange position that would be reached if the vehicle were to switch to and maintain its lowest available thrust setting for the duration of the braking burn.

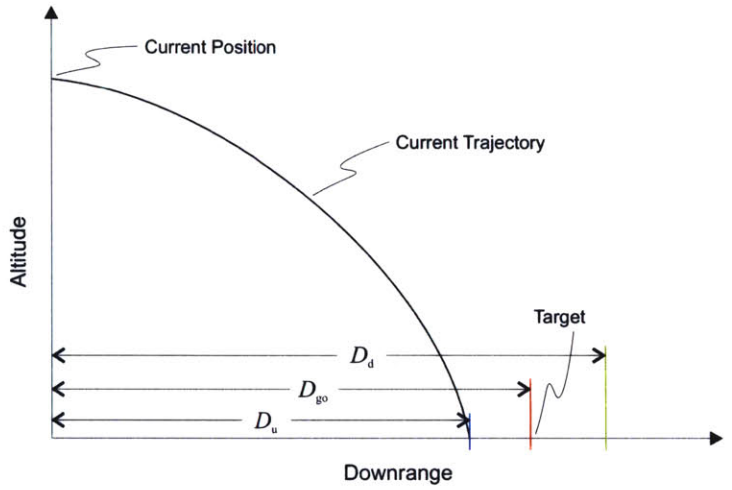

(a) Downrange-to-target and coverage limits

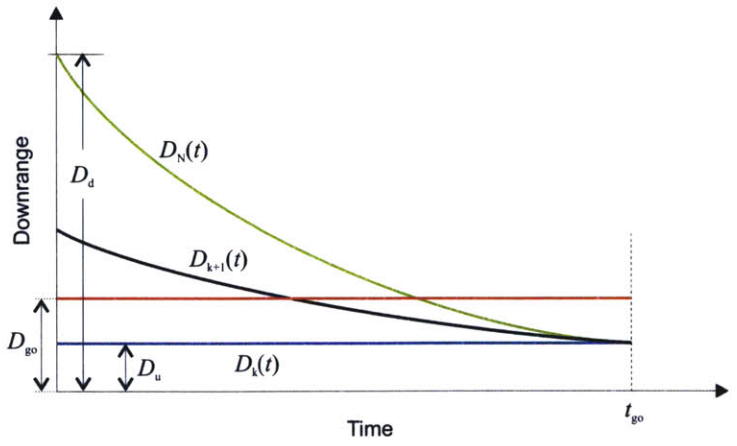

(b) Notional coverage prediction plot

Figure 3-8: Shutdown algorithm concepts

The quantities D_{go}, D_u, and D_d relate to the vehicle trajectory as shown in Figure 3-8(a). The uprange coverage limit is generally the aim point of the trajectory and, ideally, the target lies between the uprange and downrange coverage limits. If the predicted coverage limits were plotted as a function of time, the plot would resemble Figure 3-8(b). As described in Section 2.3, the predicted downrange coverage limit is monotonically decreasing with time, while the predicted uprange coverage limit is constant. The final downrange position resulting from a transition to an intermediate thrust setting also decays with time, as shown by the line labeled D_{k+1} in Figure 3-8(b). Since the steering law does not allow the vehicle to reverse its direction, D_u and D_d are always positive.

Because the vehicle has imperfect knowledge of its position, velocity, and engine performance, there is uncertainty in D_{go}, $D_1(t)$, etc., since the downrange position achieved by following a steering law converged using erroneous state, thrust, or specific impulse estimates will not match the predicted value. This uncertainty is described by a scalar quantity termed *coverage uncertainty*, which is an approximate measure of the quality of the coverage prediction. For the purposes of this thesis, an upper bound on the coverage uncertainty can be expressed as

$$\sigma_c = \sqrt{\left(\frac{\partial r_{f_{dr}}}{\partial \mathbf{x}}\sigma_{\mathbf{x}}\right)^2 + \sigma_v^2} \tag{3.73}$$

where the vehicle state $\mathbf{x}$ consists of position and velocity,

$$\mathbf{x} = \begin{bmatrix} \mathbf{r} \\ \mathbf{v} \end{bmatrix}$$

In Equation (3.73), $\frac{\partial r_{f_{dr}}}{\partial \mathbf{x}}$ is a row vector representing the sensitivity of final downrange position to changes in position and velocity, $\sigma_{\mathbf{x}}$ is a column vector containing the principle state estimate error standard deviations, and σ_v is the standard deviation of the final downrange position errors possible as a result of off-nominal engine performance. Parametric study of the nominal full thrust trajectory indicates that $\frac{\partial r_{f_{dr}}}{\partial \mathbf{x}}$ is well-approximated over a variety of conditions by

$$\frac{\partial r_{f_{dr}}}{\partial \mathbf{x}} = \begin{bmatrix} 0.204 & 1 & 0.0023 & 40.2 & 2.77 & 0.55 \end{bmatrix} \tag{3.74}$$

if $\sigma_{\mathbf{x}}$ is expressed in a local vertical-local horizontal (LVLH) coordinate frame.

Uncertainty in the final downrange position stemming from the possibility of off-nominal engine performance decreases as the remaining burn time decreases. In this thesis, the effects of off-nominal thrust and specific impulse are considered. Figure 3-9 shows the 3σ errors in the final downrange position resulting from errors in these paramters as a function of t_{go} along the nominal full thrust trajectory. Within the shutdown algorithm, σ_v is calculated via a table lookup of the data underlying Figure 3-9.

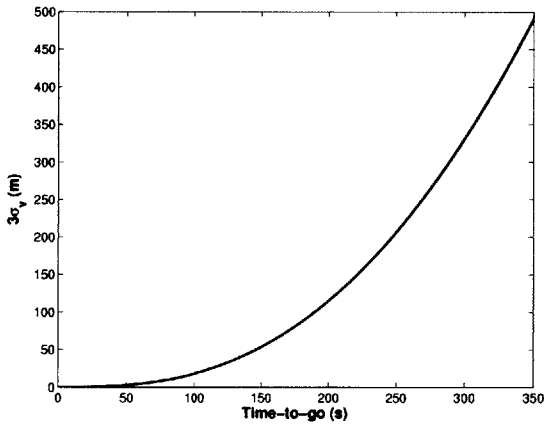

Figure 3-9: 3σ coverage uncertainty due to vehicle performance

The logic by which shutdown times are selected within the shutdown algorithm is diagrammed in Figure 3-10. The final shutdown is always set to minimize final downrange position error. Earlier shutdowns, if available, are timed to preserve coverage around the target position as far into the braking phase as possible.

Given the current state estimate, the downrange coverage provided by each available thrust level over the remainder of the braking burn can be predicted. This is represented by the "Coverage Evaluation" block in Figure 3-10. The current trajectory is predicted by integrating the vehicle equation of motion with the current steering law, and separate PEG functions, one for each remaining available thrust level, are converged along the predicted trajectory to give the predicted coverage.

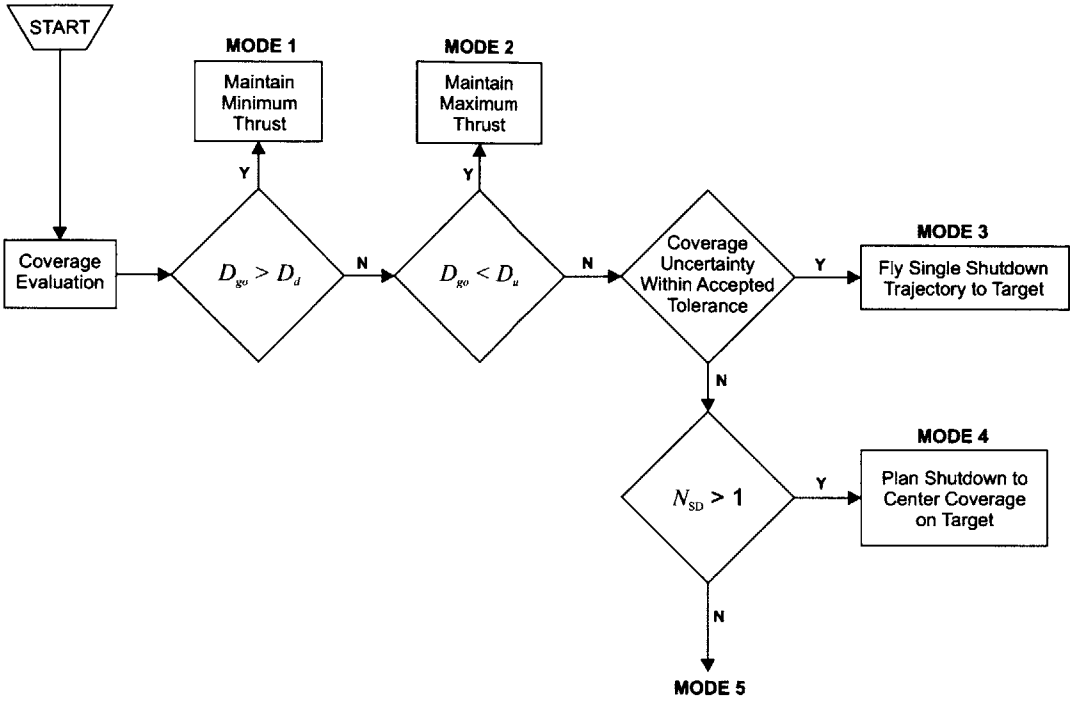

Figure 3-10: Shutdown logic block diagram

Once the predicted coverage has been evaluated, the shutdown algorithm checks for a series of conditions, always in the same order, as shown in Figure 3-10. If the target is beyond the downrange coverage limit, the vehicle transitions immediately to its lowest thrust level for the remainder of the braking phase (Mode 1). That is,

$$t_{sd_i} = t_{sd_{i+1}} = \ldots = t_{sd_{N-1}} = t \tag{3.75}$$

In general, only one shutdown is planned on each pass through the algorithm. For example, if the current thrust level is F_1, the shutdown algorithm will calculate the time at which the switch from F_1 to F_2 should occur, but not the time at which the switch from F_2 to F_3 should occur. Mode 1 is the single exception. When the target is beyond the downrange coverage limit, all shutdown times are set to effect an immediate transition to the lowest thrust level, as indicated in Equation (3.75).

If the target is uprange of the uprange coverage limit, the next shutdown time is set to a value much larger than t_{go} so that the vehicle maintains its maximum thrust for the remainder of the braking phase (Mode 2). That is,

$$t_{sd_i} = t_{go}^{+} \tag{3.76}$$

where $t_{go}^{+} > t_{go}$. Too large an ignition bias will cause the algorithm to prematurely enter Mode 1 and command an immediate transition to the lowest available thrust level, while too small an ignition bias will cause the algorithm to prematurely enter Mode 2. If the ignition bias is properly calculated, the likelihood of the shutdown algorithm entering either Mode 1 or Mode 2 early in the braking phase will be very low.

If the target is within the coverage limits, the shutdown algorithm evaluates the coverage uncertainty using Equation (3.73). If the coverage uncertainty is less than a pre-determined minimum value, the shutdown algorithm cedes control of the guidance function to a variant of PEG with an outer loop that calculates the final shutdown time to null the final downrange position error using the least amount of fuel (Mode 3), as outlined in Section 3.1.4.

If the coverage uncertainty exceeds the aforementioned minimum value, the next step is to check the number of shutdowns remaining. If the number is greater than one, the next shutdown time is calculated in the following manner. The *transition ratio* TR is defined as

$$TR(t) = \frac{D_N(t) - D_{go}}{D_{go} - D_{k+1}(t)} \tag{3.77}$$

where k denotes the current thrust level and N denotes the lowest available thrust level. The next shutdown time is calculated so that the shutdown occurs when the transition ratio has some prescribed value TR_{sd} (Mode 4):

$$t_{sd_i} = TR^{-1}(TR_{sd}) \tag{3.78}$$

This is illustrated in Figure 3-11. The value of TR_{sd} must always be greater than one to ensure that D_{go} will lie between D_{k+1} and D_N well into the future. A larger transition ratio results in an earlier shutdown time and more downrange coverage being preserved. A smaller transition ratio delays the shutdown time and preserves

uprange coverage. If only one shutdown remains, the next shutdown time is simply

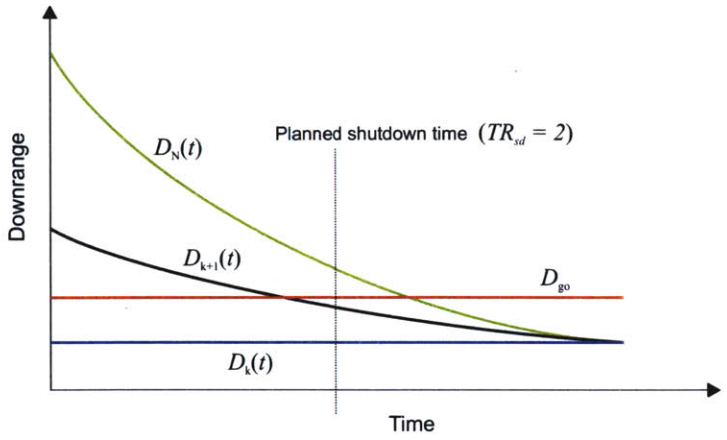

Figure 3-11: Shutting down to preserve coverage

calculated as the time at which $D_N(t)$ intercepts D_{go} (Mode 5):

$$t_{sd_i} = D_N^{-1}(D_{go}) \tag{3.79}$$

On a nominal descent, coverage would be adequate late enough into the burn to preclude the shutdown algorithm from entering either Mode 1 or Mode 2. The algorithm would enter Mode 4 as necessary to maintain coverage around the target, and eventually enter Mode 3 once the coverage uncertainty was sufficiently small. Modes 1 and 2 exist to minimize the final downrange position error in instances where coverage around the target is lost.

3.2.3 Implementation

The shutdown algorithm, as outlined in this chapter, effectively delays shutdowns to the latest possible time. This allows, as much as possible, for the navigation solution to improve before the final shutdown is executed, lowers the sensitivity of the guidance function to off-nominal vehicle performance, and lowers fuel consumption. The ignition bias is calculated in advance of the initialization of powered descent, but the logic diagrammed in Figure 3-10, as part of the overall guidance function, must be cycled periodically throughout the braking phase. While PEG is typically cycled

at least once every 2 seconds, the shutdown algorithm can be cycled less frequently, and does not need to be cycled at all early in the braking phase when the target is well within the coverage limits. In this thesis, the shutdown algorithm is initialized 4 minutes into the burn and cycled every 5 seconds. The shutdown algorithm is no longer cycled once it enters any of Modes 1, 2, or 3.

The steering function described by the equations of Section 3.1.1 can be used over a wide variety of maneuvers, but certain applications require modifications to the basic predictor-corrector loop to guarantee reliable performance. One example from the Space Shuttle program is return-to-launch-site (RTLS) abort guidance. On an RTLS abort, the main engine throttles are used to ensure that the propellant in the external tank is nearly depleted so as to assure safe separation after cutoff. Additionally, the low cutoff velocity induces coupling between the individual components of $\mathbf{v}_{go}$ as PEG is converged. These circumstances necessitate a change in the formulation of the correction equations. The details are described in Ref. [23].

Unanticipated step changes in the thrust level, which are a potential byproduct of the shutdown algorithm as formulated in this chapter, can give rise to the same type of issue in the mechanization of the linear tangent law used in this thesis. A step change in the thrust level is easily handled if it is anticipated in advance within the steering function. However, if such a change occurs without having been anticipated, that is, if it alters the thrust acceleration profile previously assumed within the steering function, it can cause an instability in the computation of $\dot{\lambda}$ which in turn causes high frequency oscillations in the steering commands. In order to keep the steering law smooth in the simulation runs described in Chapter 4, the $\mathbf{r}_{bias}$ term described in the Section 3.1.3 was left out of the implementation of PEG used to steer the vehicle. This results in a prediction error within the steering function, but its ultimate impact on the final downrange position is limited. This is discussed in further detail in Chapter 4.

As may already be apparent, there are certain parameters within the shutdown algorithm that can be tuned to affect its performance. One is the value of the ignition bias. Larger (more conservative) ignition biases cause systematically earlier

shutdowns, which is inefficient from a ΔV standpoint and results in an earlier than necessary loss of uprange coverage. Smaller ignition biases sacrifice uprange coverage when it may in fact be needed. The value of the ignition bias used in this thesis is 7.5 km, based on the results presented in Section 4.2.1, as noted earlier.

Another tuneable parameter is the minimum coverage uncertainty value required to initiate a single shutdown trajectory to the target. Too large a requirement results in a final shutdown time calculation based on a potentially inaccurate state estimate. Too small a minimum value precludes the vehicle from effectively using its final shutdown, resulting in larger final downrange position errors. The value for this thesis was chosen as 17 m, based upon the assumed navigation scenario outlined in the next chapter.

Finally, there is the dimensionless transition ratio defined by Equation (3.77), which influences shutdowns intended to preserve coverage around the target when the coverage uncertainty is high. The transition ratio used in this thesis is 1.5. With perfect navigation and vehicle performance, a larger transition ratio would keep the target within the coverage limits for longer period of time following the shutdown. However, a larger transition ratio would also leave less margin for error in the uprange direction. All else being equal, a larger transition ratio would most likely push the mean final downrange position error downrange, while a smaller transition ratio would most likely move it uprange.

Chapter 4

Guided Descent Simulation Results

It remains to assess the shutdown algorithm developed in Chapter 3 by means of a numerical simulation. A 3-DOF simulation is employed in this chapter to allow the performance of the sequential engine shutdown guidance scheme to be evaluated relative to the performance realized with either a single fixed thrust engine (worst-case) or a continuous throttle (best-case). The simulation is compact and fast, allowing Monte Carlo techniques to be leveraged to incorporate navigation and vehicle performance errors. All aspects of the simulation, including the simplifications contained within, are fully described in the first part of this chapter, with results and analyses following.

4.1 Simulation Overview

The block diagram in Figure 4-1 illustrates the structure of the braking phase simulation. The simulation is designed to model, to first order, the interaction between the navigation system, guidance system, and vehicle dynamics that would occur on an actual powered descent. It has three main components: the error models, the guidance function, and a numerical integrator. The error models are described in Sections 4.1.1 and 4.1.2, the guidance function was described in Chapter 3, and the integrator is described below.

The Moon is modeled as a non-rotating sphere of radius 1,737.4 km with a New-

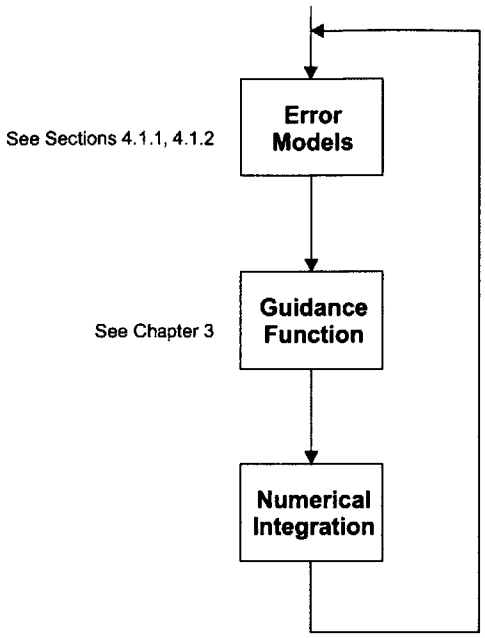

Figure 4-1: Braking phase simulation block diagram

tonian gravity field whose gravitational parameter μ is 4,902.786 km^3/s^2. (The vehicle is assumed to have perfect knowledge of this gravity field.) Gravity perturbations due to the Earth and Sun, as well as perturbations due to the oblateness of the Moon, are neglected. There is no atmosphere around the moon. The vehicle equation of motion is as given by Equation (3.3),

$$\ddot{\mathbf{r}} = \frac{F}{m}\hat{\lambda}_F + \mathbf{g} \tag{4.1}$$

This second-order vector equation is reduced to two, three-dimensional first order systems and integrated using a fourth-order Runge-Kutta scheme, with a time step $\Delta t = 0.2\ s$, to simulate the vehicle dynamics.

The simulation is initialized with the vehicle having an estimated initial altitude of 17.5 km with an estimated horizontal velocity of 1,690.54 m/s and an estimated vertical velocity of zero, as prescribed by the reference mission of Section 2.2. Generally, of course, there is some error in this estimate, and engine performance is not always nominal. At the outset of each simulated descent, a true vehicle state is randomly generated, and the vehicle's true thrust and specific impulse are randomly selected

as described in Section 4.1.2. On each pass through the simulation loop, the true vehicle state $\mathbf{x}$ (again consisting of just position and velocity) is passed to the error model, which generates an estimated state $\hat{\mathbf{x}}$ and corresponding covariance of the state estimate error. The estimated state and covariance are passed to the guidance function, which calculates the shutdown times and the steering law for the braking burn according to the guidance strategy described in Chapter 3. The true state is then propagated to the next simulation step using the guidance command calculated from the estimated state. The propagated true state is fed back to the error model, which updates the estimated state. This loop continues until the guidance function terminates the braking phase.

4.1.1 Navigation Error Model

So that the simulation runs as fast as possible and to reduce development time, a full navigation filter implementation was not included. Rather, the state estimate error — and by extension the state estimate itself — is simulated according to a model based on the results of a recent lunar landing navigation study.* The state estimate passed to the guidance function is formed by adding the state estimate error $\tilde{\mathbf{x}}$ to the true state

$$\hat{\mathbf{x}} = \mathbf{x} + \tilde{\mathbf{x}} \tag{4.2}$$

The state estimate error is modeled as a random process and is characterized by the assumed navigation instrumentation. In order for the simulation results to be valid, the random process must satisfy two criteria, namely, that its statistics be in agreement with the results of the navigation study, and that individual samples of the process resemble the actual navigation error profiles generated as part of the study.

The assumed navigation instrumentation consists of an inertial measurement unit (IMU), as well as a radar altimeter, Doppler velocimeter, and a terrain matching sensor. IMU outputs are available from the beginning of the braking phase, whereas

*carried out at the Charles Stark Draper Laboratory as part of the Lunar Access program

the other sensors provide outputs below an altitude of 5 km. The navigation error model thus has two phases. The first phase, during which the only available navigation measurements are provided by the IMU, lasts from initialization of the braking phase until the vehicle has reached 5 km altitude. The second phase covers the remainder of the braking burn, during which the state estimate is dominated by measurements from the altimeter, velocimeter, and terrain matching sensor. While the second phase of the model is somewhat optimistic, the first is fairly conservative, in that a higher altimeter activation altitude, which would improve the altitude and downrange components of the state estimate earlier in the braking phase, could be assumed.

At time $t = 0$ (or simulation step $k = 1$), the initial state estimate error vector $\tilde{\mathbf{x}}_{i_1}$ is drawn from a multivariate normal distribution with mean zero and covariance $\mathbf{P}_{i_1}$. During the first phase of the navigation error model, the error vector is subject to the applicable vehicle dynamics as well as a driving accelerometer error. Thus, the error vector is "propagated" during the first phase according to the equation

$$\tilde{\mathbf{x}}_{k+1} = \Phi\tilde{\mathbf{x}}_k + \mathbf{B}\epsilon_k \tag{4.3}$$

where the coefficients Φ and $\mathbf{B}$ are

$$\Phi = \begin{bmatrix} 1 & 0 & 0 & \Delta t & 0 & 0 \\ 0 & 1 & 0 & 0 & \Delta t & 0 \\ 0 & 0 & 1 & 0 & 0 & \Delta t \\ 0 & 0 & 0 & 1 & 0 & 0 \\ 1 & 0 & 0 & 0 & 1 & 0 \\ 1 & 0 & 0 & 0 & 0 & 1 \end{bmatrix}, \quad \mathbf{B} = \begin{bmatrix} 0 & 0 & 0 \\ 0 & 0 & 0 \\ 0 & 0 & 0 \\ \Delta t & 0 & 0 \\ 0 & \Delta t & 0 \\ 0 & 0 & \Delta t \end{bmatrix}$$

and ϵ is the random walk component of the accelerometer error. According to the accelerometer error model derived in Ref. [25], a first-order expression for the difference between the measured and true accelerations is

$$\mathbf{a}_m - \mathbf{a} = \Gamma\mathbf{a} + \mathbf{S}\mathbf{a} + \mathbf{b} + \epsilon \tag{4.4}$$

where input axis nonorthogonality and gyro-to-accelerometer misalignment errors are captured by $\mathbf{\Gamma}$, scale factor errors by $\mathbf{S}$, and bias errors by $\mathbf{b}$. Here, it is assumed that those three terms have been estimated to a high degree of accuracy within the navigation filter prior to initialization of powered descent, and thus only the random walk term is included in Equation (4.3). The 1-σ value of that error, $1.5 \times 10^{-4}\ m/s/\sqrt{s}$, comes from the Honeywell Miniature Inertial Measurement Unit specification.

During the second phase of the navigation error model, once the vehicle has passed through 5 km altitude, the state estimate error is modeled as a Gauss-Markov process. From the outset of the second phase, the state estimate error is assumed to be dominated by the new measurements and thus essentially uncorrelated with prior state estimate errors. Therefore, within the simulation, a new state estimate error $\tilde{\mathbf{x}}_{i_2}$ is drawn from a multivariate normal distribution with mean zero and covariance $\mathbf{P}_{i_2}$. The error vector is "propagated" during the second phase according to the equation

$$\tilde{\mathbf{x}}_{k+1} = e^{-\beta \Delta t} \tilde{\mathbf{x}}_k + \mathbf{w}_k \tag{4.5}$$

where $1/\beta$ is the time constant for the Gauss-Markov process and $\mathbf{w}_k$ is an uncorrelated zero-mean Gaussian sequence. The time constant β and the statistics of $\mathbf{w}_k$ are set such that the error profiles generated by the simulation are consistent with those generated as part of the lunar landing navigation study alluded to earlier:

$$\beta = \begin{bmatrix} 0.05 \\ 0.05 \\ 0.05 \\ 0.05 \\ 0.05 \\ 0.05 \end{bmatrix}, \quad E[\mathbf{w}_k \mathbf{w}_k^T] = \begin{bmatrix} 0.04 & 0 & 0 & 0 & 0 & 0 \\ 0 & 0.04 & 0 & 0 & 0 & 0 \\ 0 & 0 & 0.04 & 0 & 0 & 0 \\ 0 & 0 & 0 & 10^{-6} & 0 & 0 \\ 0 & 0 & 0 & 0 & 10^{-6} & 0 \\ 0 & 0 & 0 & 0 & 0 & 10^{-6} \end{bmatrix}$$

When simulated according to the model described in this section, the state estimate error profiles on each of the position and velocity channels are zero mean and, as required, have statistics consistent with the aforementioned lunar landing navi-

gation study. Additionally, the individual error profiles generated by the simulation are consistent with those predicted by the study. A sample error profile is shown in Figure 4-2. The covariance of the state estimate error passed to the guidance function is approximated as a function of altitude. The 1σ root mean square errors on each channel are plotted over altitude in Figure 4-3.

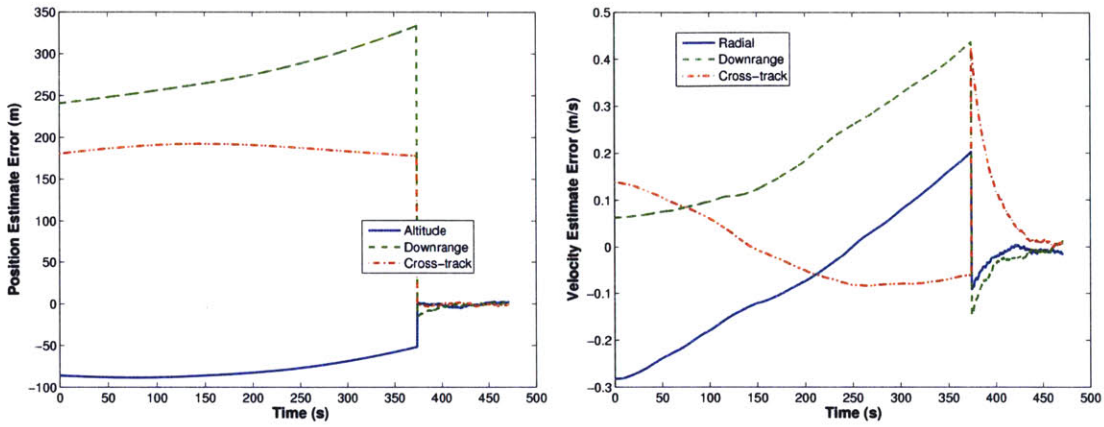

(a) Position (b) Velocity

Figure 4-2: Sample navigation error profiles

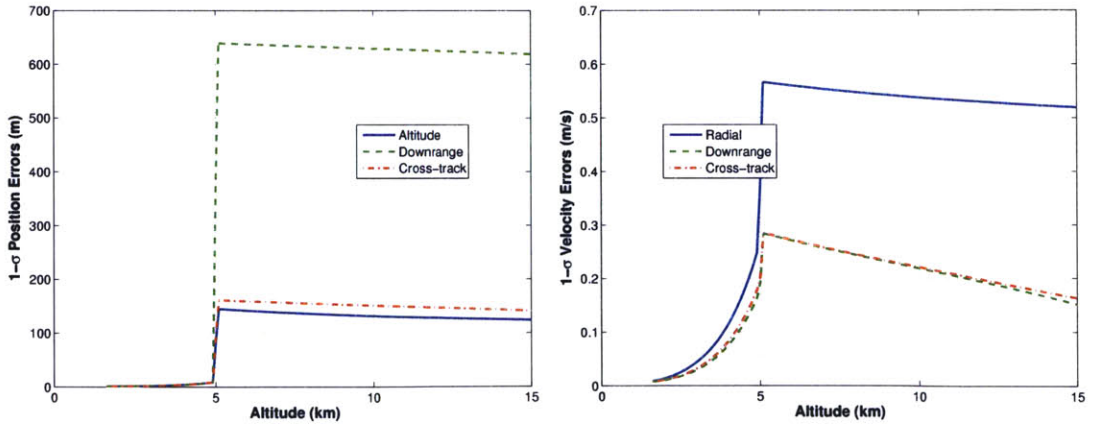

(a) Position (b) Velocity

Figure 4-3: 1-σ navigation errors as a function of altitude

4.1.2 Vehicle Performance Model

Thrust and Specific Impulse

Engine thrust and specific impulse are allowed to vary around their nominal values within the simulation. In multiple-engine simulations, both parameters are the same for each engine. In other words, on a given simulation run, all of the engines produce the same thrust and operate at the same specific impulse. Performance is not allowed to vary engine to engine. Although this is unrealistic, modeling all engines as identically performing allows the effects of off-nominal performance to be more easily analyzed.

True thrust — expressed as a fraction of rated thrust — and specific impulse are modeled as random variables described by independent, zero-mean, truncated normal distributions and are constant throughout each simulated descent. The truncation is made at ± 3 standard deviations from the mean. The statistics of each distribution are based on data from a 2004 paper describing testing of the Japanese H-2 rocket engine [26] and are given in Table 4.1.

Table 4.1: Thrust and specific impulse distributions

Variable	*Mean*	*Std. Dev.*
Fraction of Rated Thrust	1	0.0065
Specific Impulse (s)	440	3.3

Mass Estimation

The estimated mass of the vehicle is a factor in the sequential engine shutdown guidance function, because it is used within PEG to calculate the acceleration profile over the burn when a shutdown is anticipated. Since it is not possible to estimate the true fuel mass flow rate, errors build up in the vehicle mass estimate if either thrust or specific impulse is off-nominal. The estimated fuel mass flow rate $\hat{m}$ is always given by the nominal vehicle thrust divided by the nominal exhaust velocity. The magnitude of the vehicle mass estimate error grows with time according to the

difference between this estimated mass flow rate and the true fuel mass flow rate. Thus, within the simulation, the vehicle mass estimate error is propagated according to the equation

$$\tilde{m}_{k+1} = \tilde{m}_k + (\hat{\dot{m}} - \dot{m})\Delta t \tag{4.6}$$

where the term $\hat{\dot{m}} - \dot{m}$ reflects the difference between the estimated and true fuel mass flow rates.

It follows from the mission architecture assumed in Section 2.2 (descent from parking orbit) that the only opportunity for error to accumulate in the vehicle mass estimate prior to initialization of the braking phase is during the transition from the parking orbit to the transfer orbit. Until this point in the mission, the mass of the landing vehicle is assumed to be known almost perfectly, and due to the short duration of the de-orbit burn, the magnitude of the error accumulated is negligible. Therefore, at the outset of each simulated descent, the vehicle mass estimate error is initialized to zero.

4.2 Results

Given the presence of navigation uncertainty and off-nominal vehicle performance, assessing the guidance strategy presented in Chapter 3 is a probabilistic exercise. Therefore, each set of results presented in this section is associated with a set of 1,000 Monte Carlo trials of the braking phase simulation described in Section 4.1. In every case, the altitude and cross-track components of the terminal position as well as all components of the terminal velocity were tightly controlled, generally to within $\pm 10\ m$ in position and $\pm 0.05\ m/s$ in velocity, as illustrated by the histograms in Figure 4-8 (see Section 4.2.3). This was expected, since the design of PEG leaves only the final downrange position unconstrained.

Seven sets of Monte Carlo trials were carried out to study the performance of the shutdown algorithm. In order to more easily interpret those results, two additional sets of Monte Carlo trials were carried out. The first assumed a single fixed thrust

engine, meaning that the only downrange control available was via the ignition bias. The second assumed a continuously throttleable engine. The results of these two additional sets of trials are presented in Sections 4.2.1 and 4.2.2, and establish lower and upper limits, respectively, on the braking phase accuracy achievable using a sequential engine shutdown vehicle. The results of a set of trials run with the 4-engine pair, 3-thrust level configuration studied in Chapter 2 are then presented and analyzed in Section 4.2.3. Section 4.2.4 examines the effects of increasing or decreasing the number of available thrust levels, and Section 4.2.5 looks at the performance of the shutdown algorithm in instances where a plane change takes place during the braking phase.

Performance differences among the various cases boil down to the distributions of final downrange position errors and, to a lesser extent, the ΔV requirements observed in each case. One quantity used to compare performance is a linear error probable henceforth known as the *downrange error probable* (DEP). A 50% DEP of 100 m means that 50% of the trials in a given set terminated with the vehicle within ± 100 m of the target in the downrange direction.

4.2.1 Fixed Thrust Performance

As has been noted several times, the final downrange position is uncontrolled in the case of PEG-guided descent at a fixed thrust level. Therefore, a set of Monte Carlo trials of the simulation described in Section 4.1 assuming a single fixed-thrust engine yields the worst-case distribution of downrange position errors at the end of the braking phase. The terminal altitude, cross-track position, and all components of the terminal velocity are still accurately controlled. Their error distributions essentially mirror those of Figure 4-8.

A histogram of the final downrange position errors for the fixed thrust case is shown in Figure 4-4, and its statistics are summarized in Table 4.2. Notably, the distribution is centered slightly to the right of zero, and the right hand side tail of the distribution is longer than the left hand side tail. This is due to the effect of navigation errors in the cross-track direction. While altitude or downrange estimate

errors can cause final downrange position errors in either direction, errors in the cross-track direction always increase the final downrange position. The mean of the final downrange position errors is 53.8 m with a standard deviation of 2,468.2 m.

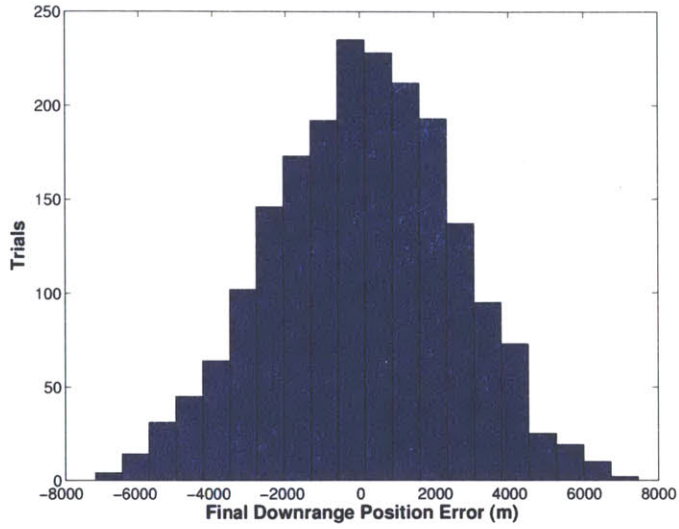

Figure 4-4: Histogram of final downrange position errors with fixed thrust

Table 4.2: Final downrange position error statistics with fixed thrust

Avg. (m)	*Std. Dev.*	*Min.*	*Max.*	50% *DEP*	95% *DEP*
53.8	2,468.2	-7,196.6	7,452.5	1,702.0	4,823.7

The fixed thrust case is also useful in gauging the relative impacts of off-nominal thrust performance, off-nominal specific impulse performance, and navigation errors on final downrange position accuracy. Figure 4-5 isolates the effects of each of these three sources of error. Figure 4-5(a) was generated with thrust varied according to the distribution in Table 4.1, while specific impulse was held at its nominal value and the vehicle was simulated as having perfect knowledge of its position and velocity. Likewise, Figure 4-5(b) was generated with only specific impulse allowed to vary from its nominal value, and Figure 4-5(c) was generated with navigation errors simulated according to the model described in Section 4.1.1 and all else nominal. Clearly, the effect of off-nominal thrust performance is dominant, but the effects of off-nominal specific impulse performance and navigation errors are significant as well.

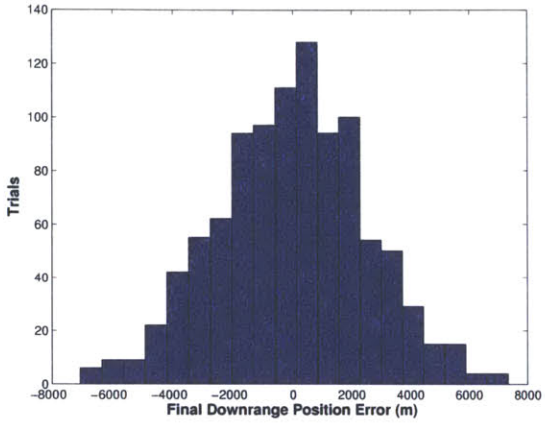

(a) Off-nominal thrust

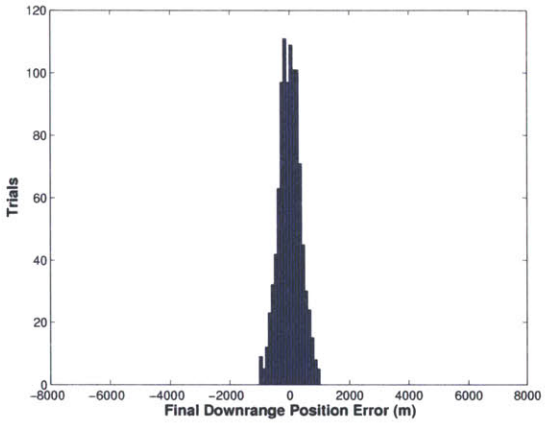

(b) Off-nominal specific impulse

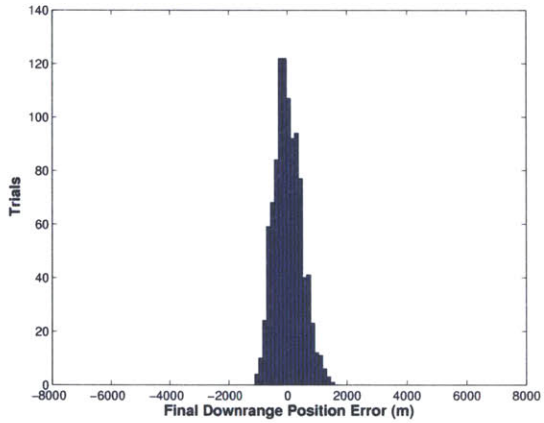

(c) Navigation errors

Figure 4-5: Individual impact of navigation and vehicle performance errors

4.2.2 Throttle Performance

In contrast to the fixed thrust case, the throttle case yields the best-case distribution of downrange position errors at the end of the braking phase. As in the fixed thrust case, errors in terminal altitude, cross-track position, and all components of the terminal velocity were distributed as they are in Figure 4-8. However, the final downrange position errors are several orders of magnitude smaller in the throttle case. A histogram of the final downrange position errors for the throttle case is shown in Figure 4-6. The final downrange position error statistics are given in Table 4.3. The throttle allows the final downrange position to be controlled to nearly the same degree of accuracy as altitude and cross-track position.

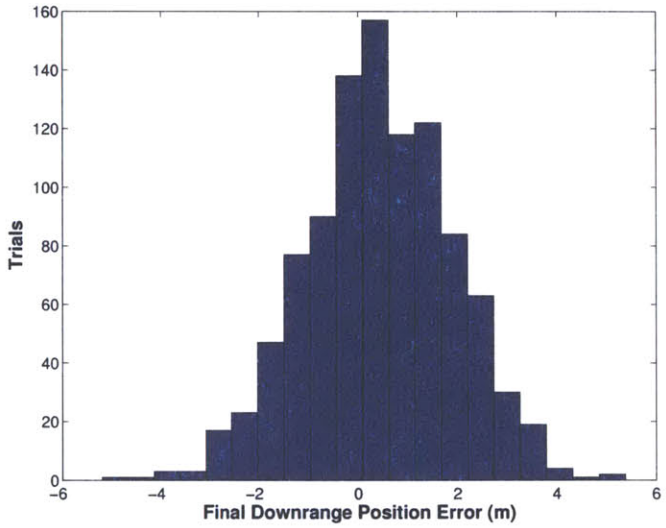

Figure 4-6: Histogram of final downrange position errors with a throttle

Table 4.3: Final downrange position error statistics with a throttle

Avg. (m)	*Std. Dev.*	*Min.*	*Max.*	50% *DEP*	95% *DEP*
0.4	1.5	-5.2	5.4	1.8	3.0

As in the sequential engine shutdown cases, the throttle case requires that the ignition point be biased uprange to prevent the vehicle from overshooting the target. However, the ignition bias for the throttle case cannot be calculated from the results of the fixed thrust case, as it was for the sequential engine shutdown cases, because

the throttle setting is adjusted continuously throughout the braking phase. It can be demonstrated that the throttle case, as implemented in this thesis, requires a substantially larger ignition bias than the 7.5 km used in the shutdown algorithm.

The scatter plot in Figure 4-7 was generated using an ignition bias of 30 km and shows final downrange position errors to be highly correlated with large negative errors in the downrange component of the initial position estimate, as indicated by the circled points on the plot. A negative error in the downrange component of the position estimate implies that the navigation estimate places the vehicle farther from the target than it actually is. This results in a commanded throttle setting that is lower than it should be, causing the vehicle to head downrange of the target. If the error in the downrange component of the position estimate remains large until additional navigation measurements become available, the required increase in the throttle setting comes too late to completely null the final downrange position error, resulting in an overshoot. The ignition bias for the throttle case must be large enough to shallow the trajectory such that the final downrange position error can be nulled out as the navigation solution improves. An ignition bias of 45 km, selected by simple trial and error, was used in the throttle case.

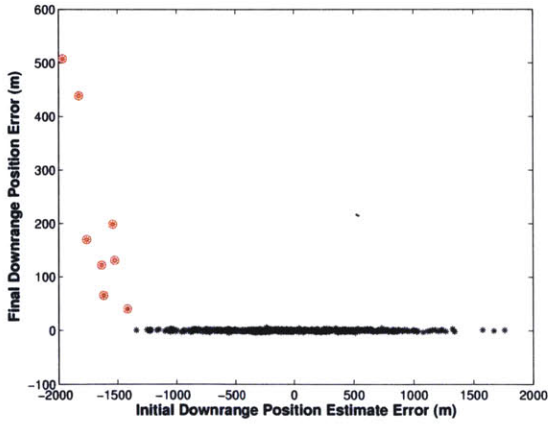

Figure 4-7: Overshoot errors under throttle guidance

The navigation scenario described in Section 4.1.1 assumes an altimeter activation altitude of 5 km. As previously noted, it is possible to activate the altimeter at a considerably higher altitude, which would decrease the root mean square of the

initial navigation errors on the downrange channel by a factor of approximately four, substantially reducing the chance of an overshoot. It is also possible to simply force the vehicle to fly at full thrust for most of the braking phase, then activate the throttle computation once the coverage uncertainty is low. That approach, however, removes most of the ΔV advantage enjoyed by the throttle case.

The results summarized in Table 4.3 do not indicate that the use of a throttle guarantees meter-level braking phase accuracy. The relatively low fidelity of the simulation used to obtain these results precludes their interpretation as a prediction of actual system performance. Rather, as the fixed thrust results are a worst-case reference, the throttle results provide a best-case reference against which the performance of the shutdown algorithm can be judged.

4.2.3 Sequential Engine Shutdown Performance: Base Case

Each of the seven sets of Monte Carlo trials carried out in assessing the performance of the shutdown algorithm assumes the baseline vehicle, but the number of available thrust levels and the orbital plane of the target vary from set to set. A "base case", consisting of the 3-thrust level engine configuration studied in Chapter 2 and a braking phase target in the nominal orbital plane of the vehicle, is presented and analyzed in this section. The base case engine configuration is reproduced from Table 2.3 as Table 4.4.

Table 4.4: Baseline vehicle with 3 thrust levels

Avail. Thrust Levels	F_{max} (N)	F_{min}	*Engine Thrust*	*No. Engine Pairs*
3	227,500	113,750	28,437	4

As alluded to earlier, the altitude and cross-track components of the final position as well as all components of the final velocity were accurately controlled by the direction of thrust in the base case. Histograms of the errors in each component of the final position and velocity, except for the downrange component of the final position, are shown in Figure 4-8. A histogram of the errors in the downrange component of

the final position is shown in Figure 4-9, and their statistics are given in Table 4.5. The base case results conform to expectations relative to the results of both the fixed thrust case and the throttle case. In terms of standard deviation, 50% DEP, and 95% DEP, downrange accuracy in the base case is better than it is in the fixed thrust case by a factor of approximately 35, but worse than it is in the throttle case by a factor of approximately 50.

Table 4.5: Final downrange position error statistics with 3 thrust levels

Thrust Levels	*Avg. (m)*	*Std. Dev.*	*Min.*	*Max.*	50% *DEP*	95% *DEP*
3	57.1	73.7	-374.4	397.1	51.5	196.2

Figure 4-10(a) shows how the times of the two available shutdowns were distributed in the base case. Trials in which only one or no shutdowns took place are not distinguished in the figure. Figure 4-10(b) shows how the navigation update times (i.e., the times at which the vehicle passed through 5 km altitude) and total burn times were distributed. By and large, the first shutdown was executed soon after the vehicle passed through 5 km altitude, and the second shutdown took place sometime between 1–2 minutes prior to the end of the braking phase.

In the vast majority of the base case trials (i.e., 97.5%), the last active mode of the shutdown algorithm was Mode 3. In other words, the typical base case trial saw the coverage uncertainty decrease rapidly as the vehicle passed through 5 km altitude. Once the coverage uncertainty became sufficiently small, the vehicle transitioned to a single shutdown trajectory aimed at the desired final downrange position. Since the most efficient single shutdown trajectory generally involved thrust levels F_2 and F_3 (the second-lowest and lowest thrust levels, respectively), the first shutdown served simply to reduce the thrust level from F_1 to F_2. This indicates that the assumed navigation suite, as modeled, can provide a sufficiently good position estimate early enough in the descent to support accurate landings, and that the value of the ignition bias is appropriate given the assumed navigation suite and the vehicle performance model specified in Table 4.1. Navigation system performance and the size of the

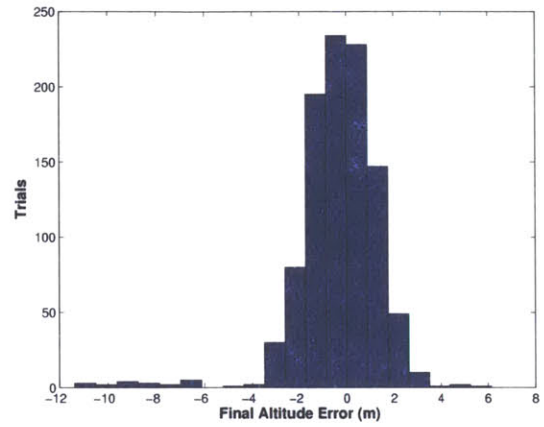

(a) Altitude

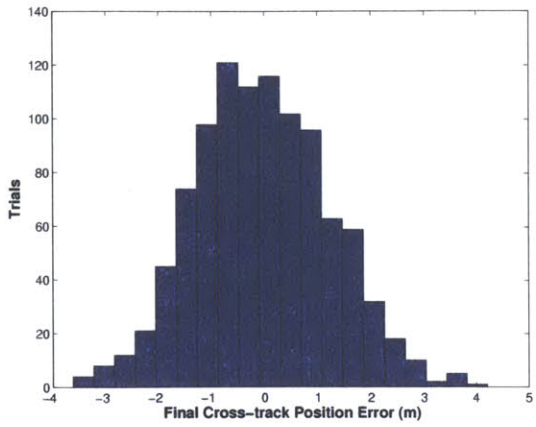

(b) Cross-track position

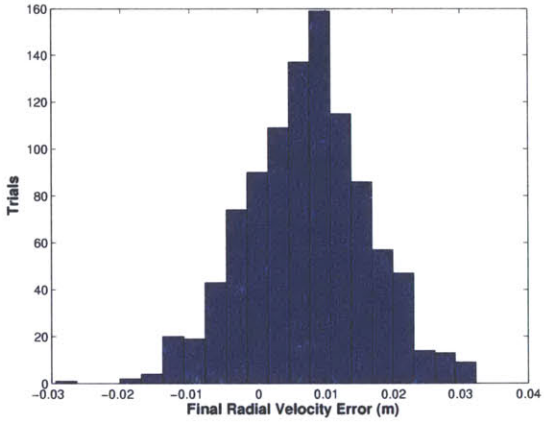

(c) Radial velocity

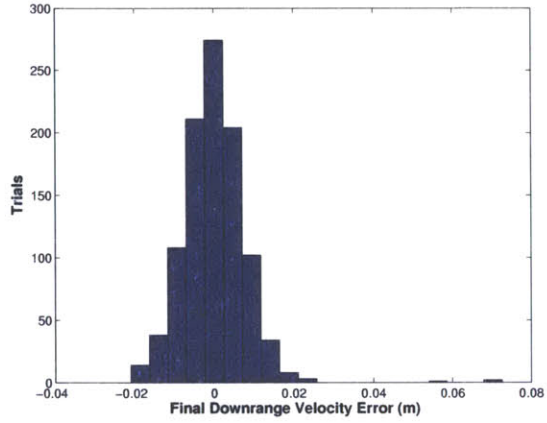

(d) Downrange velocity

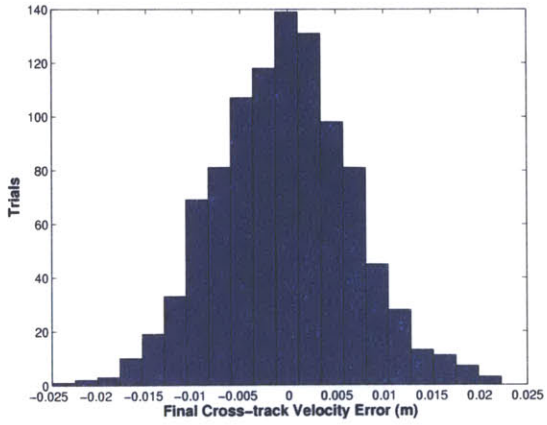

(e) Cross-track velocity

Figure 4-8: Final position and velocity error histograms with 3 thrust levels

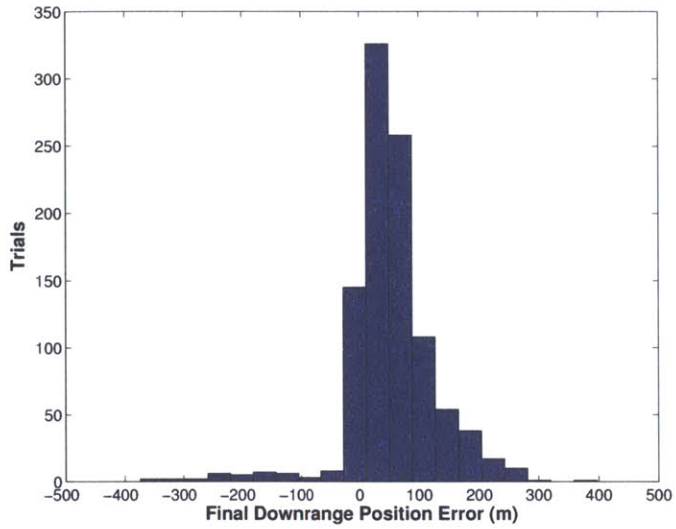

Figure 4-9: Histogram of final downrange position errors with 3 thrust levels

ignition bias are the primary determinants of the vehicle's ability to maintain coverage around the braking phase target.

The principal sources of error in the final downrange position are navigation errors and off-nominal thrust and specific impulse performance. The relative impact of each of these error sources was examined in Section 4.2.1. The difference between the accuracy observed in the throttle case and that observed using sequential engine shutdown is accounted for by the inability of the vehicle to effect any control over its final downrange position once the last shutdown has been executed.

Although the coverage uncertainty is generally low by the time the last shutdown takes place, small navigation and vehicle performance errors persist through the remainder of the braking phase. After the final shutdown, the vehicle continues to command the direction of thrust so as to null errors in the altitude and cross-track components of the final position as well as errors in the final velocity. That action affects the final downrange position, and cannot be anticipated in the calculation of the final shutdown time. Thus, the final downrange position actually achieved diverges from the value predicted at the time of the final shutdown. The effect of compensating for residual navigation errors and off-nominal vehicle performance tends to extend the final downrange position, hence the right-heavy distribution in Figure 4-9.

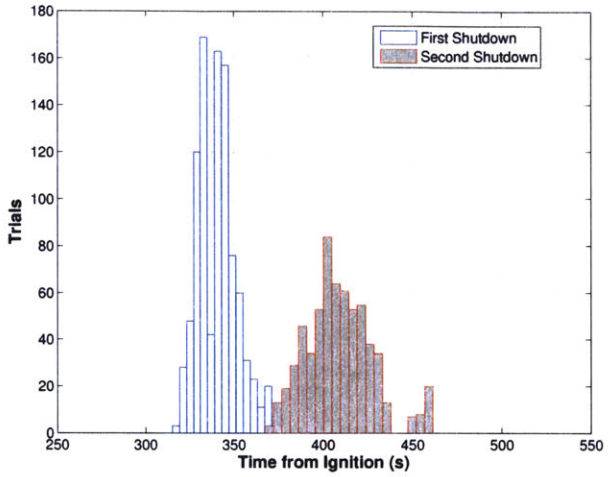

(a) Shutdown times

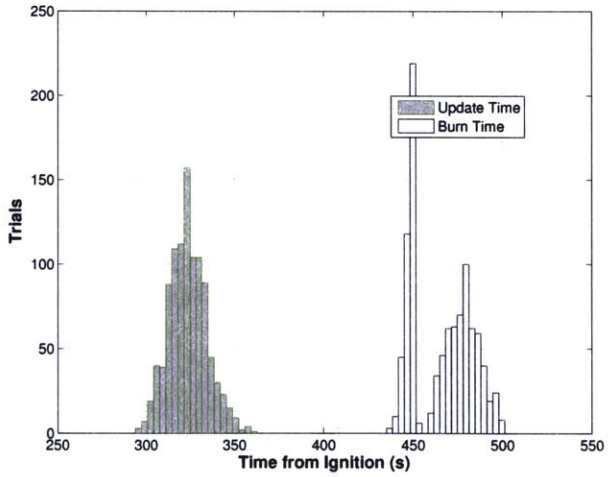

(b) Navigation update and burn times

Figure 4-10: Shutdown time, navigation update time, and burn time histograms

4.2.4 Changing the Number of Thrust Levels

The base case involved one possible engine configuration. Its results leave the matter of the impact of increasing or decreasing the number of available thrust levels unresolved. To address this, three sets of Monte Carlo trials apart from the base case were carried out, using engine configurations with 2, 4, and 5 available thrust levels (and thus 1, 3, and 4 available shutdowns, respectively). As in the base case, the engine configuration in each of these cases corresponds to a configuration from Table 2.3. The engine configurations are reproduced in Table 4.6.

Table 4.6: Baseline vehicle with 2, 4, and 5 thrust levels

Avail. Thrust Levels	F_{max} (N)	F_{min}	*Engine Thrust*	*No. Engine Pairs*
2	227,500	113,750	56,875	2
4	227,500	91,000	22,750	5
5	227,500	97,500	16,250	7

In each case, as expected, control of the altitude and cross-track components of the terminal position, as well as all components of the terminal veloctity, was quite good, with no appreciable differences compared to the base case results. Downrange accuracy, as well as ΔV performance, improved as the number of thrust levels was increased, and degraded as that number was decreased. Histograms of the final downrange position errors observed in each case are shown in Figures 4-11, 4-12, and 4-13. The statistics of these errors are given in Table 4.7.

Downrange accuracy in the 2-level case was surprisingly good in light of the hypothesis that it might suffer with only a single shutdown available. The relative success of the 2-level case can be mostly attributed to the performance of the navigation suite. As observed in the base case, the 5 km navigation update came sufficiently early to allow a single shutdown to null much of the final downrange position error. The results of the 2-level case are also perhaps the most convincing indication the ignition bias was properly calculated.

The downrange accuracy with 2 thrust levels, however good, was still noticeably worse than the downrange accuracy observed in the base case. This has to do with

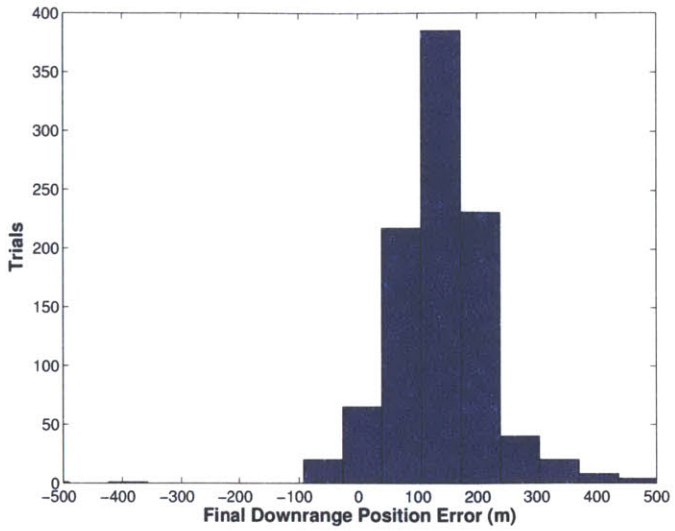

Figure 4-11: Histogram of final downrange position errors with 2 thrust levels

the duration of the portion of the braking phase taking place after the final shutdown in the 2-level case being, on average, 30% longer than it was in the base case. Since error in the final downrange position builds up after the final shutdown has been used, one would expect the magnitude of these errors to be roughly proportional to the burn time remaining after the final shutdown, if all else were constant. Indeed, the standard deviation of the final downrange position errors in the 2-level case was approximately 30% higher than it was in the base case.

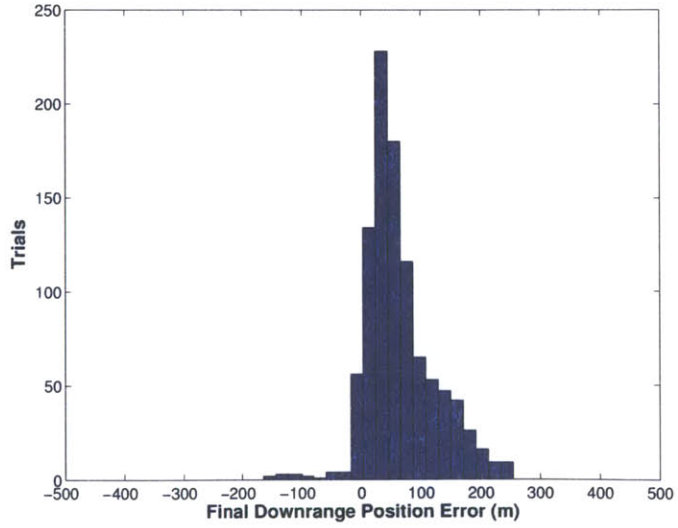

Figure 4-12: Histogram of final downrange position errors with 4 thrust levels

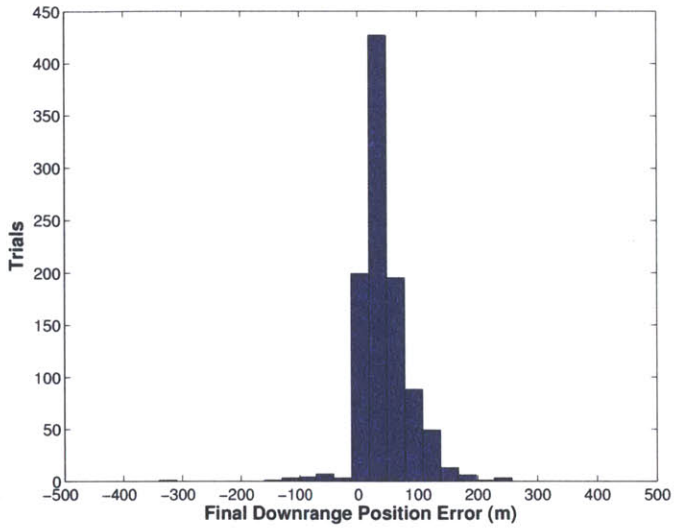

Figure 4-13: Histogram of final downrange position errors with 5 thrust levels

Accuracy in the 4- and 5-level cases was improved over the base case. In both cases, the standard deviation of the final downrange position errors was smaller than in the base case, though the average error increased very slightly in the 4-level case. The difference in these two cases was not the burn time remaining after the final shutdown, which on average was almost the same as it was in the base case, but the magnitude of the thrust level used during that portion of the burn. In the 4-level case, the majority of the trials ended with the vehicle at a thrust level of 136,500 N, versus 113,750 N in the 2-level and base cases. In the 5-level case, the majority of the trials ended with the vehicle at a thrust level of either 130,000 N or 162,500 N. At higher thrust levels, smaller deviations from the steering profile predicted at the time of the final shutdown are required to maintain altitude, cross-track, and velocity accuracy, and thus their effect on the final downrange position is decreased. The improvement observed in the 4- and 5-level cases had less to do with the number of thrust levels available than it did with the magnitudes of those thrust levels.

The average ΔV requirements in each case were: 1,836.5 m/s in the 2-level case, 1,820.3 m/s in the 3-level case, 1,815.8 m/s in the 4-level case, and 1,813.1 m/s in the 5-level case. It was asserted in Chapter 2 that the most fuel efficient single-shutdown trajectory involves the two available thrust levels nearest in each direction to the constant thrust setting that would yield the desired final downrange position.

Table 4.7: Final downrange position error statistics: 2, 4, and 5 thrust levels

Thrust Levels	*Mean (m)*	*Std. Dev.*	*Min.*	*Max.*	50% *DEP*	95% *DEP*
2	142.7	92.0	-556.0	767.5	139.0	281.2
4	64.5	57.9	-165.1	254.4	53.7	176.8
5	43.8	41.5	-339.7	257.0	37.9	119.4

It follows from this assertion that the average ΔV requirements would be ordered with the 2-level case having the highest ΔV requirement and the 5-level case having the lowest, and the average ΔV requirements observed in the simulations support that conclusion.

There does appear to be a point of diminishing returns with respect to the ΔV requirement as the number of thrust levels increases. With each added thrust level, there is a smaller decrease in the interval between thrust levels. Hence there is an almost negligible difference in ΔV requirement between the 4- and 5-level cases. Of course, it should be noted that the total range of ΔV requirements observed over all sets of trials involving the shutdown algorithm is rather narrow.

4.2.5 Changing the Orbital Plane

Chapter 2 alluded to the possible need to accomodate large lateral offsets in the target position during the braking phase via a plane change. Several sets of Monte Carlo trials were carried out to test the performance of the shutdown algorithm under descent scenarios involving a change in the inclination of the vehicle's orbital plane. The results are summarized in Figure 4-14 and Table 4.8, and were obtained using the base case engine configuration (see Table 4.4), with the indicated inclination change commanded at initialization of powered descent. The shutdown algorithm underlying these results is exactly as it was in the in-plane cases detailed in the previous two sections.

Although not shown here, there is a significant drop in downrange accuracy when the magnitude of the commanded inclination change is increased beyond 6°. This implies that a realistic limit on the lateral offset that can be accomodated is approx-

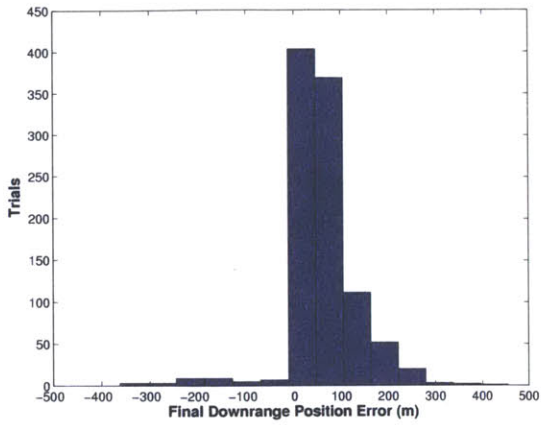

(a) 1° inclination change

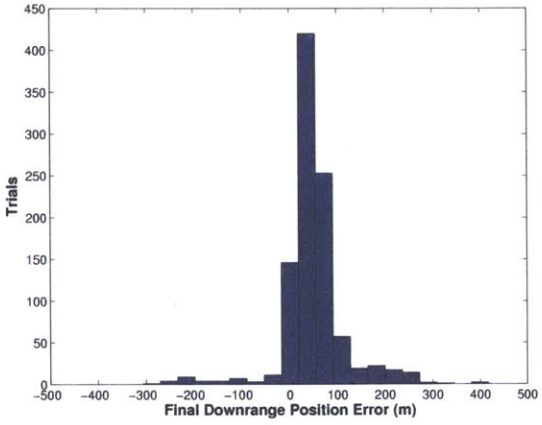

(b) 3° inclination change

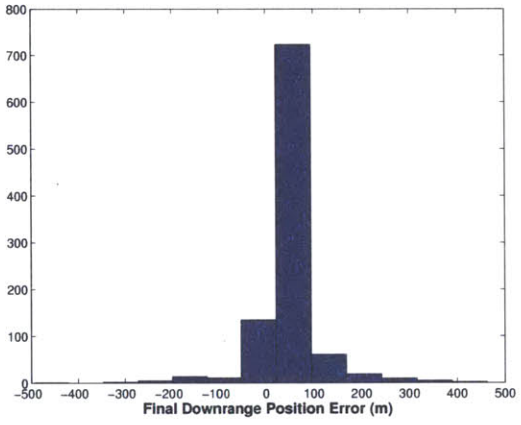

(c) 5° inclination change

Figure 4-14: Final downrange position errors with plane changes

Table 4.8: Final downrange position error statistics with plane changes

Δi (deg)	*Mean* (m)	*Std. Dev.*	*Min.*	*Max.*	50% *DEP*	95% *DEP*
1	61.0	77.1	-362.6	804.6	55.0	206.6
3	50.5	68.0	-306.7	416.8	49.0	206.5
5	46.9	90.0	-1,255.3	463.2	49.8	172.3

imately $\pm 50\ km$, if the inclination change is commanded at the outset of the braking phase. That limit decreases if the inclination change is commanded later in the braking phase. The drop in accuracy is foreshadowed by the small number of outlying trials (those in which the final downrange position error exceeds the 6σ value) observed in each of the plane change cases. The number of outlying trials, which are not included in Figure 4-14 or Table 4.8, increased from just 1 with $\Delta i = 1°$ to 9 with $\Delta i = 5°$.

For inclination changes greater than 6°, the shallowing of the descent trajectory causes downrange coverage to decay in such a way that the available shutdowns are used relatively early in the braking phase. Final downrange position control is lost before the navigation update becomes available, resulting in large final position errors. The average ΔV requirements for the plane change cases are higher than for the in-plane cases presented in Sections 4.2.3 and 4.2.4, but for inclination changes below 6°, the difference is only 20–30 m/s.

4.3 Discussion

Of the adjustable parameters within the shutdown algorithm discussed at the end of Chapter 3, it appears that the most important is the size of the ignition bias. It was observed in simulation trials that too large an ignition bias can increase final downrange position errors by as much as an order of magnitude. Another of the adjustable shutdown algorithm parameters, the minimum coverage uncertainty required to transition to a single shutdown trajectory, was well-tuned, as evidenced by the large number of trials in each case that terminated on such a trajectory. The final adjustable parameter, the transition ratio defined by Equation (3.77), had little observable impact on the simulation results, since the simulated navigation system performance precluded a frequent need for the coverage-preserving shutdowns that the transition ratio influences.

In Section 3.2.3, it was noted that the exclusion of the $\mathbf{r}_{bias}$ term in the implementation of PEG used to steer the vehicle results in a difference between the final

downrange position predicted within PEG prior to the end of the braking phase and the final downrange position actually achieved.[†] The magnitude of this prediction error decreases as the remaining burn time decreases, as illustrated in Figure 4-15, which contains a plot of the prediction error over t_{go} along the nominal full-thrust trajectory. The prediction error resulting from the exclusion of the $\mathbf{r}_{bias}$ term is another potential source of final downrange position error. However, as Figure 4-15 indicates, the prediction error over the applicable range of remaining burn times is almost negligible. At 5–15 m, it accounts for only a very small percentage of the magnitude of the final downrange position errors shown in Figure 4-9.

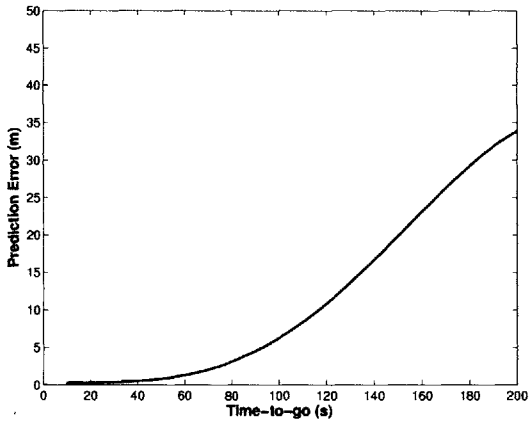

Figure 4-15: Prediction error along the nominal full thrust trajectory

The results presented in this chapter suggest that the shutdown algorithm is capable of doing a fair job of limiting downrange dispersions under the assumed (and in some ways optimistic) navigation scenario. Some ability to accomodate lateral changes in the target position during the braking phase is retained using sequential engine shutdown. Although the shutdown algorithm did not limit downrange dispersions to the extent observed in the throttle case, the errors observed in the sequential engine shutdown cases are small enough to allow them to be nulled out over the terminal descent.

[†]In fact, some prediction error is always present, but its magnitude is larger when the $\mathbf{r}_{bias}$ term is excluded.

Chapter 5

Conclusions

5.1 Thesis Summary

Chapter 1 began with an overview of past lunar landing efforts, including recent proposals. The notion of sequential engine shutdown was introduced and its application to lunar descent was motivated. The problem to be solved in the thesis was formulated and the relevant previous work available in the literature was discussed.

Chapter 2 defined a baseline vehicle and reference mission and used them to explore the use of sequential engine shutdown. Of particular importance was the analysis of the downrange control provided by sequential engine shutdown and the effects of shutdown timing on that control. Chapter 3 detailed a guidance strategy for a sequential engine shutdown vehicle. The theory underlying the linear tangent guidance law was presented, and the use of both throttling and engine shutdowns for final downrange position control was discussed. A shutdown algorithm, consisting of a pre-calculated ignition bias and a heuristic governing the use of available engine shutdowns, to be used in conjunction with a mechanization of the linear tangent law, was then developed.

In Chapter 4, the shutdown algorithm was assessed against guidance schemes relying on fixed thrust and continuously throttleable engines. A statistical picture of the performance of each guidance scheme was obtained via Monte Carlo trials of a simulation intended to capture, to first order, the interaction between the descent

propulsion system, the navigation filter, and the guidance function. Errors in the final downrange position and, to a lesser extent, average ΔV requirements, formed the basis for comparison. The results are summarized in Tables 5.1 and 5.2.

Table 5.1: Summary of final downrange position error statistics

Downrange Control	*Mean (m)*	*Std. Dev.*	*Min.*	*Max.*	*50% DEP*	*95% DEP*
None	53.8	2,468.2	-7,196.6	7,452.5	1,702.0	4,823.7
Shutdowns (1)	142.7	92.0	-556.0	767.5	139.0	281.2
Shutdowns (2)	57.1	73.7	-374.4	397.1	51.5	196.2
Shutdowns (3)	64.5	57.9	-165.1	254.4	53.7	176.8
Shutdowns (4)	43.8	41.5	-339.7	257.0	37.9	119.4
Throttle	0.4	1.5	-5.2	5.4	1.8	3.0

Table 5.2: Summary of average ΔV requirements

Downrange Control	*Mean* ΔV *(m/s)*
None	1,775.6
Engine Shutdowns (1)	1,836.5
Engine Shutdowns (2)	1,820.3
Engine Shutdowns (3)	1,815.8
Engine Shutdowns (4)	1,813.1
Throttle	1,789.5

As expected, the performance of the shutdown algorithm fell between that observed with a fixed thrust engine and a throttle. In terms of standard deviation and 50% and 95% downrange error probables, downrange accuracy using the shutdown algorithm was better than in the fixed thrust case by a factor of approximately 35. Accuracy in the throttle case was better than that observed using the shutdown algorithm by an additional factor of approximately 50. The throttle case also had a slightly lower ΔV requirement than any of the cases involving sequential engine shutdown.

Among the four engine configurations that relied upon shutdown algorithm, accuracy improved and the ΔV requirement was lowered as the number of thrust levels was increased. As noted in Chapter 4, both of these trends were primarily attributable to a favorable navigation scenario, a properly calculated ignition bias, and the mag-

nitudes of the available thrust levels, rather than to the number of available thrust levels. The results suggest that a relatively simple shutdown logic can yield good accuracy and ΔV performance, provided the performance of the navigation system is adequate.

5.2 Future Work

The shutdown algorithm, as formulated in Chapter 3, plans shutdowns in such a way that the steering law must effectively be re-converged under a different assumed thrust acceleration profile each time a shutdown takes place. An alternative way of handling engine shutdowns within the guidance function is to define a reference trajectory such that the braking phase target would be obtained under nominal conditions via shutdowns executed at pre-determined times. The shutdown times would then be revised throughout the braking phase to compensate for navigation errors and off-nominal vehicle performance. The advantage of this approach is that every shutdown would be automatically anticipated within the steering function. It would not, however, eliminate the possibility of discontinuities in the steer law, since a large change in any of the shutdown times would produce the same effect on the steer law as an unanticipated shutdown does under the shutdown algorithm outlined in Chapter 3.

Coverage would evolve differently over the braking phase under this alternative approach. The uprange coverage limit would no longer be constant, as it is shown to be in Figures 2-8 and 3-8(b). Rather, it would move toward the target position throughout the burn. The downrange coverage limit would decay more slowly than illustrated in the aforementioned figures, and would always intersect the uprange coverage limit at t_{go}. Despite this difference, the basic goal of the shutdown algorithm — maintaining coverage around the target — would remain unchanged.

This thesis did not address the possibility of an engine failure during the braking phase. That possibility was addressed, however, as part of the recent Draper/MIT Crew Exploration Vehicle concept exploration and refinement study (see Ref. [22]). The analysis suggested that when large thrusters like those postulated in this thesis

are used, the only realistic course of action, when one engine in a pair fails, is to shut down the other member of the pair. For a sequential engine shutdown vehicle, this would entail an immediate loss of uprange coverage. It may be possible to make some allowance in the shutdown algorithm for this contingency, which would presumably increase the robustness of the algorithm at the expense of accuracy.

Additionally, in previous studies, the terrain matching sensor has been assumed to be fixed to the vehicle, not gimballed. Thus, rapid changes in attitude during the braking phase or a slower sweep through a large attitude interval have the potential to cause difficulties in pointing this sensor. Given the high level of performance expected of the terrain matching sensor, this could pose a potentially significant technical hurdle.

A number of steps can and should be taken to refine the simulation results presented in Chapter 4. The first is to move to a 6-degree of freedom simulation with a higher fidelity Moon model. Because the rotational motion of the vehicle is not modeled in this thesis, the vehicle follows the steering commands perfectly within the simulation. Where the shutdown algorithm is involved, this is a major simplification, since the shutdown algorithm allows discontinuities in the steering commands. It is less unrealistic when a fixed thrust engine or a throttle is assumed. For obvious reasons, a full navigation filter implementation should be part of any future simulation. Additionally, a more realistic engine shutdown model is needed. Engine shutdowns are not instantaneous, and the degree of precision to which the timing of a shutdown can be controlled was not investigated as part of this work.

Sequential engine shutdown, as defined in this thesis, is only one in a broad spectrum of approaches to the lunar descent problem involving multiple constant thrust engines. It could be augmented, for example, by the ability to restart engines one or more times, or by the addition of a small range of vernier throttleability around each discrete thrust level. Such a vernier capability, which could be provided by pulsing the attitude control system or by gimballing the main engines, offers perhaps the most straightforward method of improving landing accuracy using sequential engine shutdown.

Bibliography

[1] D. R. Woods, "A review of the Soviet lunar exploration programme," *Spaceflight*, vol. 18, pp. 273–290, July/Aug. 1976.

[2] R. C. Hall, "Project Ranger: A chronology," Jet Propulsion Laboratory, California Institute of Technology, Pasadena, CA, Tech. Rep. JPL/HR-2, 1971.

[3] R. J. Parks, "Surveyor I mission report," Jet Propulsion Laboratory, California Institute of Technology, Pasadena, CA, Technical Report 32-1023, Aug. 1966.

[4] J. J. Ribarich, "Surveyor spacecraft landing accuracy," in *AIAA Guidance, Control and Flight Dynamics Conference*, Huntsville, AL, Aug. 14–16, 1967, paper AIAA-67-544.

[5] A. R. Klumpp, "Apollo lunar descent guidance," *Automatica*, vol. 10, pp. 133–146, Mar. 1974.

[6] G. Elverum, P. Staudhammer, J. Miller, and A. Hoffman, "The descent engine for the lunar module," in *AIAA 3rd Propulsion Joint Specialist Conference*, Washington, DC, July 17–21, 1967, paper AIAA-67-521.

[7] R. H. Battin, *An Introduction to the Mathematics and Methods of Astrodynamics*, revised ed. Reston, VA: AIAA, 1999.

[8] W. J. Larson and L. K. Pranke, Eds., *Human Spaceflight: Mission Analysis and Design.* New York: McGraw Hill, 2000.

[9] C. N. D'Souza, "An optimal guidance law for planetary landing," in *AIAA Guidance, Navigation, and Control Conference*, New Orleans, LA, Aug. 11–13, 1997, paper AIAA-1997-3709.

[10] J. Vilja, "Rocketdyne advanced propulsion systems overview," in *AIAA/ASME/SAE/ASEE Joint Propulsion Conference and Exhibit*, Seattle, WA, July 6–9, 1997, paper AIAA-1997-3309.

[11] D. R. Jenkins, *Space Shuttle: The History of Developing the National Space Transportation System*, 2nd ed. Indian Harbour Beach, FL: Dennis R. Jenkins, 1996.

[12] G. P. Sutton and O. Biblarz, *Rocket Propulsion Elements*, 7th ed. New York: John Wiley and Sons, Inc., 2001.

[13] D. F. Lawden, *Optimal Trajectories for Space Navigation.* London: Butterworth and Co., Ltd., 1963.

[14] G. W. Cherry, "E Guidance — a general explicit, optimizing guidance law for rocket-propelled spacecraft," MIT Instrumentation Laboratory, Cambridge, MA, Tech. Rep. R-456, Aug. 1964.

[15] S. Ueno and Y. Yamaguchi, "3-Dimensional near-minimum fuel guidance law of a lunar landing module," in *AIAA Guidance, Navigation, and Control Conference and Exhibit*, Portland, OR, Aug. 9–11, 1999, paper AIAA-1999-3983.

[16] A. Axelrod, M. Guelman, and D. Mishne, "Optimal control of interplanetary trajectories using electrical propulsion with discrete thrust levels," *AIAA Journal of Guidance, Control, and Dynamics*, vol. 25, no. 23, pp. 932–939, Sept./Oct. 2002.

[17] M. Vasile and R. Floberghagen, "Optimal trajectories for lunar landing missions," in *AAS/GSFC International Symposium*, ser. Advances in the Astronautical Sciences. San Diego: Univelt, Inc., 1998, pp. 133–139.

[18] A. M. Hawkins, "Constrained trajectory optimization of a soft lunar landing from a parking orbit," Master's thesis, Massachusetts Institute of Technology, Cambridge, 2005.

[19] S. Zimmer, C. Ocampo, and R. Bishop, "Incorporating observability into trajectory optimization," in *AIAA/AAS Spaceflight Mechanics Meeting*, Copper Mountain, CO, Jan. 23–27, 2005, paper AAS 05-132.

[20] ——, "Finite burn trajectory optimization including observability with discrete measurements," in *AIAA/AAS Astrodynamics Specialists Conference*, Lake Tahoe, CA, Aug. 7–11, 2005, paper AAS 05-334.

[21] ——, "Decreasing semimajor axis uncertainty through trajectory design," in *AIAA/AAS Astrodynamics Specialists Conference*, Lake Tahoe, CA, Aug. 7–11, 2005, paper AAS 05-333.

[22] "Concept exploration and refinement study: Final report," Prepared for NASA Exploration Systems Mission Directorate, The Charles Stark Draper Laboratory, Inc., Sept. 2005.

[23] R. L. McHenry, T. J. Brand, A. D. Long, B. F. Cockrell, and J. R. Thibodeau, "Space Shuttle ascent guidance, navigation, and control," *The Journal of the Astronautical Sciences*, vol. 27, no. 1, pp. 1–38, Jan./Mar. 1979.

[24] A. E. Bryson and Y.-C. Ho, *Applied Optimal Control.* Chicago: Stallion Publishing, 1987.

[25] S. C. Paschall, "Mars entry navigation performance analysis using monte carlo techniques," Master's thesis, Massachusetts Institute of Technology, Cambridge, 2004.

[26] D. M. Lineberry, H. W. Coleman, and R. Sekita, "Uncertainty analysis of staged combustion LOX LH_2 rocket engine hot firing tests," in *AIAA/ASME/SAE/ASEE Joint Propulsion Conference and Exhibit*, Rio de Janeiro, Brazil, July 11–14, 2004, paper AIAA-2004-4002.